Chemical Engineering Journal 482 (2024) 149045

Contents lists available at ScienceDirect

Chemical Engineering Journal

journal homepage: www.elsevier.com/locate/cej

Improving the propylene selectivity in the methanol-to-olefins reaction over CIT-17, a SAT-type molecular sieve

Faisal H. Alshafei [a,b], Stacey I. Zones [c], Mark E. Davis [a,*]

[a] Chemical Engineering, California Institute of Technology, Pasadena, CA 91125, United States
[b] Department of Chemical Engineering, Massachusetts Institute of Technology, Cambridge, MA 02139, United States
[c] Chevron Energy Technology Company, 100 Chevron Way, Richmond, CA 94802, United States

ARTICLE INFO

Keywords:
CIT-17
Methanol-to-olefins
Silicoaluminophosphates
SAT
Selectivity
Propylene

ABSTRACT

Small-pore, cage-containing molecular sieves exhibit high selectivities toward light olefins in the methanol-to-olefins (MTO) reaction. However, the ability to alter the olefins product selectivities while achieving high carbon efficiency remains a challenge for this complex reaction network. Here, the synthesis, characterization, and catalytic testing of several SAT-type molecular sieves: SAPO (CIT-17), MgAPO (STA-2), and CoAPO (STA-2) are reported. Several CHA- (e.g., SAPO-34, MgAPO-34, and CoAPO-34) and AEI-type (e.g., SAPO-18, MgAPO-18, and CoAPO-18) molecular sieves are synthesized and tested for comparisons. The SAT materials exhibit high propylene selectivities ranging from approximately 35 % to 50 % in the MTO reaction. Remarkably high propylene-to-ethylene ratios (P/E) ranging from 1.64 to 4.17 are achieved, depending on the reaction conditions and molecular sieve properties. These P/E ratios are higher than those obtained from CHA- (P/E = 0.91–1.31) and AEI-type (P/E = 2.10–2.34) materials at complete or near-complete methanol conversion. The enhanced P/E ratios exhibited by the SAT-type catalysts with low silicon contents (e.g., CIT-17 (Si/T-atom = 0.083)) are ascribed to the time-on-stream delay in the maturation of aromatic species that are comprised primarily of tri- and tetra-methylbenzenes. The results from this study demonstrate the subtle cooperativity between the narrow SAT cage (cage-defining ring (CDR) size of 6.6 Å) and low acidity of CIT-17. These factors together create a conducive microenvironment that facilitates the conversion of methanol-to-propylene by promoting the olefins cycle, particularly in early stages of the reaction, and reducing the contribution of the aromatics cycle.

1. Introduction

Ethylene (E; $C_{2=}$) and propylene (P; $C_{3=}$) are two of the most important building blocks in the petrochemical industry as they are key in the synthesis of a wide array of polymers (e.g., polyethylene and polypropylene) and fine chemicals [1,2]. However, a global propylene shortage is predicted as demand is expected to outstrip supply due to the rapidly growing demand for propylene along with the low propylene yields that are achieved in steam cracking and fluid catalytic cracking (FCC) processes [3–5]. These market dynamics have paved the road for on-purpose propylene production technologies such as propane dehydrogenation, butenes metathesis, Fischer-Tropsch-to-olefins, and methanol-to-olefins (MTO) to fill this widening gap between supply and demand [6–11].

MTO is one of the most promising non-petroleum routes to produce light olefins (e.g., ethylene, propylene, and butenes (B)), since methanol can be produced from syngas ($CO/CO_2/H_2$), which can be obtained from several abundant feedstocks or alternative carbon raw materials, including natural gas, coal, biomass, CO_2, and municipal waste [12–16]. Molecular sieves containing Brønsted acid sites are the catalysts of choice in methanol (MeOH) conversion processes, such as MTO, or more broadly, methanol-to-hydrocarbons (MTH), with ZSM-5 (MFI structure) and SAPO-34 (CHA) being the two catalysts deployed industrially [17]. Molecular sieve topology is one of the most important parameters that influences the MTO catalytic performance and regulates product distribution [18–24]. However, the strength, distribution/proximity (i.e., presence of paired sites), location, amount, and the nature of the acid sites can also contribute toward the observed catalytic behavior [25–32]. Indeed, controlling product selectivity in MTO is an intricate interplay of many parameters that are either inherent to the catalyst or governed by reaction conditions (e.g., temperature, weight hourly space velocity (WHSV), etc.) [33–36].

* Corresponding author.
E-mail address: mdavis@cheme.caltech.edu (M.E. Davis).

https://doi.org/10.1016/j.cej.2024.149045

Available online 24 January 2024

In light of the pronounced industrial significance of this reaction, considerable efforts have been devoted to unraveling its underlying mechanism. It is now widely accepted that methanol conversion reactions over acidic, molecular sieve-based catalysts proceed via an indirect hydrocarbon pool (HP) mechanism, comprising of two coexisting yet competing catalytic cycles (i.e., dual cycle): an aromatics-based cycle and an olefins-based cycle [17,37–39]. In the aromatics cycle, which typically predominates in small-pore, cage-type molecular sieves (e.g., CHA, AEI, and ERI), poly-methylbenzenes (MB) act as pivotal active HP species that undergo repeated methylation and dealkylation reactions to form ethylene, propylene, and/or butenes, depending on the reaction pathway (paring or side-chain) [21,40–43]. On the other hand, in the olefins cycle, which is more prominent in channel-type molecular sieves (e.g., MFI and TON), olefins repeatedly undergo methylation and β-scission reactions to form primarily C_{3+} products [44]. These two cycles are connected via hydrogen transfer and cyclization reactions that convert the olefin-based species to aromatic species. Based on several previous studies, ethylene is recognized as a terminal product of the aromatics cycle, and as such, it can be used as an indicator of the propagation of this cycle whereas the selectivity of 2-methylbutane and 2-methyl-2-butene (i.e., ratio of ethene to 2-methylbutane and 2-methyl-2-butene) or the combined selectivities of higher aliphatic species (e.g., C_{4+}) are often used as indicators of the prevalence of the olefins cycle [30,45].

Because propylene is a product formed in both cycles, enhancing its selectivity (i.e., improving the propylene-to-ethylene (P/E) ratio) from a material design standpoint is typically achieved in one of two approaches. The first and more conventional approach involves the utilization of 10- or 12-member ring (MR) zeolites with high Si/Al ratios that impart low acid site numbers in the catalysts, in order to suppress the formation of aromatic species and promote the olefins cycle; the second approach involves the use 8-MR molecular sieves with cages larger than CHA (e.g., AEI, DDR, ITE, and RTH) to accommodate higher substituted methylbenzenes, which in turn are associated with enhanced propylene production via the aromatics cycle [18,21,23,46–50]. Some of the catalysts discussed in the literature that exhibit pronounced propensity for propylene formation (and fall under the aforementioned 'first/conventional' approach), include, high-silica ZSM-5 (Si/Al = 216), which gives a propylene selectivity of approximately 51 % and a P/E of 12.1 [49]; high silica EU-1 zeolite (Si/Al = 200), which achieves a propylene selectivity of 52 % and a P/E of 15 [51]; and high-silica beta zeolites (Si/Al = 136–340), which provides a propylene selectivity of 49.7–58.3 % [52]. Although each of these catalysts exhibits an exceptionally high P/E ratio alongside a high propylene selectivity, their relatively large cavities and pore sizes lead to substantial yields of various C_{4+} hydrocarbons (typically 30+%). A distinctive advantage that small-pore, cage-containing molecular sieves have over 10- or 12-MR zeotypes lies in their ability to confine the size of the products capable of diffusing out of their pores (albeit with a potential trade-off of accelerated deactivation), thus, achieving higher light olefins selectivities. Indeed, achieving a more constrained product distribution provides the potential of simplifying downstream separations while maintaining a high carbon efficacy towards targeted products.

Our group has reported on several small-pore, cage-containing materials that enhance the propylene selectivity over CHA-type molecular sieves (e.g., SAPO-34 and SSZ-13), including SAPO-18 (AEI), steamed and unsteamed SSZ-39 (AEI), zeolite RTH, SSZ-28 (DDR), and ITQ-3 (ITE) [18,19,28,29,53]. However, none of these materials achieved a P/E ratio higher than ca. 2.5 at our reaction conditions (temperature of 400 °C and $WHSV_{MeOH}$ of 1.3 h^{-1}). This constraint likely arises from the fact that even though larger cages accommodate higher substituted methylbenzenes (MBs) (e.g., penta- (5 MB) and hexa-methylbenzenes (6 MB)), once these MBs form, it becomes difficult to regulate (or eliminate) the formation of lower substituted methylbenzenes (e.g., tri- and tetra-methylbenzenes), which are associated with the formation of ethylene. As such, even though small-pore, cage-type molecular sieves with large cages can enhance the propylene selectivity in MTO over CHA-type molecular sieves, the P/E ratios achieved in such materials appear restrained and are significantly lower than those obtained in medium- or large-pore zeolites with high Si/Al ratios.

Recently, Yang et al. [54] reported on the synthesis and catalytic testing of several small-pore $AlPO_4$-14/SAPO-14 (AFN) molecular sieves with low acid site densities (Si/T = 0–0.022) (T = Si + Al + P). In spite of their short lifetime (shorter than 20 min), AFN-type molecular sieves achieved remarkably high P/E ratios of 3.1–4.1. These high P/E ratios were attributed to the combination of low acid site density of the SAPO-14 catalyst along with the structural features of the ultra-small cage of AFN, which enabled control over the formation of key HP species. We also recently investigated the MTO behavior of several ERI-type molecular sieves (e.g., SAPO-17, SSZ-98, UZM-12, ERI-type zeolites) [27]. ERI has one of the narrowest cages active for MTO (cage-defining ring size of 6.75 Å), which can also accommodate polymethylbenzenes. We showed that increasing the acid site density and strength of ERI-type catalysts enhances the ethylene-to-propylene ratio (E/P = 0.7–1.9) quite considerably. This enhancement in E/P ratio correlated with how fast the ERI materials accumulated active HP aromatic species as a function of Si/Al or Si/T-atom ratio. Indeed, by varying the Brønsted acidity of the catalysts, we were able to influence how quickly each ERI catalyst transitioned from an early-stage C_{3+}-rich regime (indicative of the olefins cycle) to a later-stage $C_{2=}$-rich regime (indicative of the aromatics cycle).

Here, we investigate the catalytic behavior of several SAT-type molecular sieves with the aim of improving the P/E ratio in MTO. The SAT structure consists of double six-membered rings (D6Rs), cancrinite (CAN) cages, and elongated narrow cages (CDR size of 6.6 Å) that are interconnected via elliptical 8-MRs (Fig. S1). SAT has been previously prepared by hydrothermal synthesis in the presence of bisquinuclidinium-butane (DiQ-C_4), bis-diazabicylcooctane-butane (DiDABCO-C_4), and bis-diazabicylcooctane-pentane (DiDABCO-C_5), leading to the formation of several aluminophosphate-based materials, including, $AlPO_4$, MgAPO, and ZnAPO, which are denoted herein as STA-2 [55–57]. However, the silicoaluminophosphate (SAPO) version of SAT has not been synthesized in a pure form, as SAPO-SAT was previously observed to crystallize with AFX impurities (as evidenced in the powder X-ray diffraction patterns of the formed products) [56]. In this work, we demonstrate for the first time the synthesis of SAPO-SAT (CIT-17) without AFX impurities and characterize this material using a battery of characterization techniques outlined in the next section. We compare the performance of the SAT-type molecular sieves (e.g., CIT-17, MgAPO, and CoAPO) to CHA- (e.g., SAPO-34, MgAPO-34, and CoAPO-34) and AEI-type (SAPO-18, MgAPO-18, and CoAPO-18) molecular sieves (Fig. 1), to identify material and structural properties that enhance propylene selectivity (i.e., P/E ratio) in small-pore, cage-containing molecular sieves. Partially reacted samples (after 5 min of reaction) were dissolved in hydrofluoric (HF) acid to extract and analyze the occluded organic components to identify differences between the compositions and concentrations of the entrained HP species formed during reaction. The identification of these species assists in understanding the observed differences in MTO behavior between these three frameworks.

2. Experimental

The CHA-, AEI-, and SAT-type molecular sieves investigated in this work were synthesized based on previously reported (albeit with slight modifications) or newly developed procedures. Detailed synthesis procedures of the organic structure-directing agents (OSDAs) used here are also provided. The moisture contents of the solid sources were determined by temperature-gravimetric analysis (TGA).

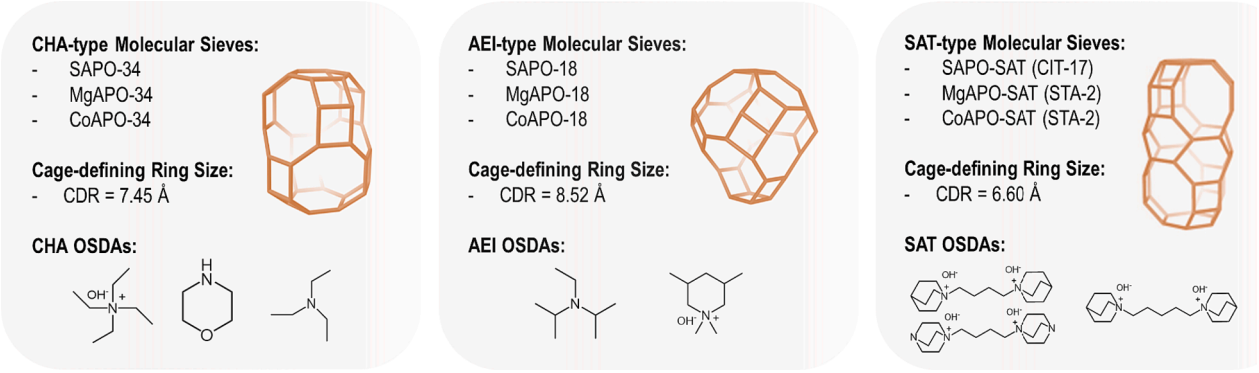

Fig. 1. Cages within the molecular sieves investigated in this work, their cage-defining ring (CDR) sizes, and the organic structure-directing agents (OSDAs) used for the syntheses of these three frameworks (CHA, AEI, and SAT). Each framework in this work is prepared as at least one SAPO, one MgAPO, and one CoAPO-type sample.

2.1. Materials

All materials, unless otherwise noted, were used as-received without further purification from the stated vendors: aluminum hydroxide (Barcroft 250, SPI Pharma), pseudoboehmite alumina (Catapal B, VISTA), phosphoric acid (H_3PO_4; Macron, 85 %), colloidal silica Ludox AS-40 (Sigma Aldrich, 40 %), fumed silica (Cab-O-Sil, ACROS), cobalt (II) acetate tetrahydrate (Sigma Aldrich, 98 %), cobalt (II) sulfate hydrate (Sigma Aldrich), magnesium acetate tetrahydrate (Sigma Aldrich, 98 %), 1,4-diazabicylco[2.2.2]octane (DABCO) (Sigma Aldrich, 99 %), 1,4-dibromobutane (Sigma Aldrich, 99 %), 1,5-dibromopentane (Sigma Aldrich, 97 %), quinuclidine (Alfa Aesar, 97 %), diethyl either (VWR, 98 %), methanol (Sigma Aldrich, 99.9 %), and acetone (Fisher Chemical).

2.2. OSDA syntheses

CHA-type molecular sieves (SAPO-34, MgAPO-34, and CoAPO-34) were synthesized using morpholine (Thermo Scientific, 99 %) and tetraethylammonium hydroxide (TEAOH) (Sigma Aldrich, 35 % in H_2O) as OSDAs. A sample containing both CHA and AEI (denoted as CHA/AEI or SAPO-34/18) was synthesized using triethylamine (Sigma Aldrich, 99.5 %) as an OSDA. Triethylamine and TEAOH are known to crystalline CHA (e.g., SAPO-34) but have also been used in the synthesis of CHA/AEI intergrowths, depending on the gel composition and synthesis conditions [58–61]. AEI-type molecular sieves (SAPO-18, MgAPO-18, and CoAPO-18) were synthesized using diisopropylethylamine (DIPEA) (Sigma Aldrich) and 1,1,3,5-tetramethylpiperdinium hydroxide (TMPOH, Sachem). SAT-type molecular sieves (SAPO-SAT (CIT-17), MgAPO-SAT (STA-2), CoAPO-SAT (STA-2)) were synthesized using bisquinuclidinium-butane (DiQ-C_4), bisquinuclidinium-pentane (DiQ-C_5), and bis-diazabicylcooctane-butane (DiDABCO-C_4).

2.2.1. Bisquinuclidinium-butane (DiQ-C_4)

DiQ-C_4 was prepared from the reaction of quinuclidine and 1,4-dibromobutane. In a typical synthesis, quinuclidine (100 mmol) was mixed with 150 cm^3 of methanol and stirred at room temperature for a few minutes. The solution was then heated to 45 °C in an oil bath. After reaching 45 °C, 1,4-dibromobutane (35 mmol) was added dropwise to the quinuclidine-containing solution while stirring. After adding 1,4-dibromobutane, the reaction mixture was heated to 80 °C and refluxed for 5–6 days. Methanol was then evaporated using a rotary evaporator, and the solid product was filtered and washed with methanol, diethyl ether, and acetone. Following this, the solid was dried under vacuum at room temperature for 6–8 h. The OSDA was then converted to its hydroxide form, and its concentration was determined by titration as described in the Ion Exchange and Titration Section. The ^{13}C NMR spectrum of the DiQ-C_4 is shown in Fig. S2.

2.2.2. Bisquinuclidinium-pentane (DiQ-C_5)

DiQ-C_5 was prepared from the reaction of quinuclidine and 1,5-dibromopentane. In a typical synthesis, quinuclidine (100 mmol) was mixed with 150 cm^3 of acetone and stirred at room temperature for a few minutes. The solution was then heated to 45 °C in an oil bath. After reaching 45 °C, 1,5-dibromopentane (35 mmol) was added dropwise to the quinuclidine-containing solution while stirring. After adding 1,5-dibromopentane, the reaction mixture was heated to 80 °C and refluxed for 7 days. Acetone was then evaporated using a rotary evaporator, and the solid product was filtered and washed with diethyl ether and acetone. Following this, the solid was dried under vacuum at room temperature for 6–8 h. The OSDA was then converted to its hydroxide form, and its concentration was determined by titration as described in the Ion Exchange and Titration Section. The ^{13}C NMR spectrum of the DiQ-C_5 OSDA is shown in Fig. S2.

2.2.3. Bis-diazabicylcooctane-butane (DiDABCO-C_4)

DiDABCO-C_4 was prepared from the reaction of 1,4-diazabicyclo [2.2.2]octane (abbreviated herein as DABCO) and 1,4-dibromobutane. In a typical synthesis, DABCO (600 mmol) was mixed with 150 cm^3 of methanol and stirred at room temperature for a few minutes. The solution was then heated to 45 °C in an oil bath. After reaching 45 °C, 1,4-dibromobutane (75 mmol) was added dropwise to the DABCO-containing solution while stirring. After adding 1,4-dibromobutane, the reaction mixture was heated to 80 °C and refluxed for 6 days. Methanol was then evaporated using a rotary evaporator, and the solid product was filtered and washed with methanol, diethyl ether, and acetone. Following this, the solid was dried under vacuum at room temperature for 6–8 h. The OSDA was then converted to its hydroxide form, and its concentration was determined by titration as described in the Ion Exchange and Titration Section. The ^{13}C NMR spectrum of the DiDABCO-C_4 OSDA is shown in Fig. S2.

2.2.4. Ion Exchange and Titration

If required by the molecular sieve synthesis procedure, the OSDAs described above were ion exchanged into their hydroxide forms by first dissolving the organic salts in DI water and then adding DOWEX™ Monosphere™ 550A hydroxide ion-exchange resin. Specifically, for every 100 mmol of OSDA in the halide form, approximately 300 cm^3 (by volume) of resin and 500 cm^3 of DI water were added. The mixture was then stirred for 24 h at room temperature. After 24 h, the resin was separated by filtration and the process repeated a second time. The quantification of the concentration of the OSDA, now in the hydroxide form, was performed using a Mettler Toledo DL22 Potentiometric pH meter. Five readings were taken for each OSDA concentration, and these values were then averaged and used for gel calculations. OSDAs in the hydroxide form are abbreviated with a $(OH)_2$ annotation (e.g., DiQ-C_4-

$(OH)_2$) whereas OSDAs in the halide (bromide) form are abbreviated with a $(Br)_2$ annotation (e.g., DiQ-C_4-$(Br)_2$).

2.3. Molecular sieve syntheses

2.3.1. CHA-type molecular sieves

Several CHA-type molecular sieves were synthesized or provided to us for comparison to the SAT samples. SAPO-34–1 was kindly provided by Mitsubishi and was characterized in this work. SAPO-34–2 was synthesized according to a method outlined in our previous work with a gel molar composition of 1 Al_2O_3: 1 P_2O_5: 0.075 SiO_2: 3 TEAOH: 50 H_2O [18,26]. It's characterization data were shown previously [18]. SAPO-34–3 was synthesized with a gel molar composition of 0.985 Al_2O_3: 1 P_2O_5: 0.4 SiO_2: 2 morpholine: 60 H_2O [62]. In a typical synthesis, a desired amount of pseudoboehmite was stirred in 50 % of the required deionized (DI) water for approximately 3 h. Then, phosphoric acid was added dropwise to the alumina slurry and the solution was stirred for another 2 h. After stirring, fumed silica was added along with the remaining DI water. The mixture was left to stir for 1 h before adding the OSDA (morpholine). This mixture was stirred overnight before being placed in a Teflon-lined Parr reactor (23 cm^3) and heated in a static oven to 200 °C for 48 h. Both MgAPO-34 and CoAPO-34 were synthesized based on methods outlined previously [18,63,64]. Their characterization results were also previously reported by our group [18].

2.3.2. CHA/AEI-type molecular sieve

SAPO-34/18 was synthesized with a gel molar composition of 1 Al_2O_3: 0.9 P_2O_5: 0.05 SiO_2: 3.5 triethylamine: 40 H_2O [65]. In a typical synthesis, a desired amount of pseudobohoemite and DI water were stirred for 3 h. Then, a desired amount of phosphoric acid was added along with fumed silica. This mixture was stirred for 3 h before triethylamine was added. Following the addition of the OSDA, the mixture was stirred for 2 h and then transferred to a stainless-steel Teflon-lined Parr reactor (23 cm^3) and heated in a rotating oven (55–60 rpm) to 180 °C for 24 h.

2.3.3. AEI-type molecular sieves

Several AEI-type molecular sieves were synthesized for comparison to the SAT samples. SAPO-18–1 was synthesized with a gel molar composition of 1 Al_2O_3: 0.96 P_2O_5: 0.055 SiO_2: 1.62 diisopropylethylamine: 50 H_2O [66]. In a typical synthesis, a solution of phosphoric acid and DI water was added to aluminum hydroxide hydrate (Barcroft) and the mixture was stirred overnight. Then, fumed silica was added to this mixture followed by the OSDA. The gel was stirred for an additional 2 h before being placed in a Teflon-lined Parr reactor (23 cm^3) and heated in a static oven to 160 °C for 10 days. SAPO-18–2 was synthesized using a similar procedure as SAPO-18–1, but with a slightly different gel composition (1 Al_2O_3: 0.9 P_2O_5: 0.2 SiO_2: 1.6 diisopropylethylamine (DIPEA): 50 H_2O). To obtain a pure AEI product, the H_3PO_4/OSDA ratio was adjusted in the aforementioned gel. SAPO-18–3 was synthesized using a similar gel as SAPO-18–2 but with a higher Si content (1 SiO_2). Both MgAPO-18 and CoAPO-18 were synthesized based on methods outlined in our previous work [18]. Their characterization were also previously reported by our group [18].

2.3.4. SAT-type molecular sieves

MgAPO-SAT and CoAPO-SAT were typically synthesized with a gel molar composition of 0.45–0.5 Al_2O_3: 0.45–0.55 P_2O_5: 0.025–0.1 Mg (or Co): 0.4 $R_A(OH)_2$ (R_A = DiQ-C_4 or DiDABCO-C_4): 40–75 H_2O [55,56]. This gel composition was inspired by the reported gel for STA-2. In a typical synthesis, aluminum hydroxide (Barcroft), magnesium or cobalt (II) acetate, phosphoric acid, and DiQ-C_4 or DiDABCO-C_4 in the hydroxide form were sequentially added to a Teflon-liner containing deionized (DI) water. The prepared gel, following stirring overnight, was transferred to a stainless-steel autoclave and heated at 190 °C in a rotating (or a static) oven for 2–3 days. In a few cases (before loading), a small amount of STA-2 seed (1 wt%) was added to the gel mixture. In a few other examples, a small amount of Si was added in addition to cobalt to form CoAPSO-type materials. In these examples, the OSDA concentration was lowered from 0.4 to 0.27 (to mimic the conditions typically used for the synthesis of CIT-17). Tables S1-S3 include summary tables of the syntheses gels and conditions attempted for making SAT-type molecular sieves and the resultant products as determined by Powder X-ray Diffraction (PXRD).

The synthesis of CIT-17 (SAPO-SAT) was attempted over a wide range of conditions: 0.44–0.5 Al_2O_3: 0.44–0.5 P_2O_5: 0.05–0.4 SiO_2: 0.16–0.33 $R_B(OH)_2$ (R_B = DiQ-C_4, DiQ-C_5, or DiDABCO-C_4): 0–0.11 $R_B(Br)_2$: 40–75 H_2O. In a typical synthesis, a desired amount of phosphoric acid (H_3PO_4) was mixed with an appropriate amount of DI water, and the mixture was stirred for 10 mins. Next, the aluminum source (Barcroft) was weighed separately and added to this mixture. This gel was allowed to homogenize for 3–4 h before adding fumed silica. Following the addition of the silica source, the OSDA was added, and the gel was aged at room temperature for 20–24 h before being heated to 180–200 °C in a rotating (55–60 rpm) or a static oven at autogenous pressures for 3–5 days. All CIT-17 materials were prepared in 23 cm^3 stainless steel Parr autoclaves with Teflon liners. In a few cases (before loading), a small amount of CIT-17 seed (1 wt%) was added to the gel mixture (albeit the synthesis of CIT-17 does not require the presence of a seed). A complete summary of the attempted synthesis conditions and the resultant products is outlined in Tables S1-S3.

The best crystallized CIT-17 materials were prepared using the following gel composition: 0.48–0.5 Al_2O_3: 0.45–0.5 P_2O_5: 0.05–0.15 SiO_2: 0.17–0.23 $R_A(OH)_2$ (R_A = DiQ-C_4, DiQ-C_5, or DiDABCO-C_4): 40 H_2O. It was observed that as the Al/P ratio approaches unity (by increasing the P concentration), the OSDA content ought to be on the higher end of the aforementioned gel range to obtain pure or near-pure CIT-17. Furthermore, when DiQ-C_5 is used as an OSDA, the amount of OSDA (concentration) can be increased up to 0.27 in the above gel without forming impurities. The two major impurities encountered during the synthesis of CIT-17 are AFX (as reported previously; typically, when the Si content is high or the OSDA concentration is high) and CIT-16P (typically, when the OSDA concentration is high). CIT-16P, which we recently reported on, is a disordered SAPO phase that transforms to ERI following the removal of the OSDA [67].

2.4. Product recovery and thermal treatment

Once the above syntheses were completed, each material was washed three to four times with DI water (50 cm^3 each time) and once with acetone (50 cm^3). After each wash, materials were recovered by centrifugation at 3500+ rpm (Eppendorf model 5810 R). After washing, all samples were dried in air overnight at 100 °C. Following drying, all materials were thermally treated (in ceramic calcination boats) under flowing breathing-grade air in a Nabertherm DKN400 muffle furnace. Materials were initially heated to 150 °C at a heating rate of 1 °C/min and held for 3 h before being heated to 580 °C (again at a heating rate of 1 °C/min) and held for 12 h to ensure complete combustion of any remaining organic structure-directing agents (OSDAs).

2.5. Characterization

Powder X-ray diffraction (PXRD/XRD) patterns were obtained on a Rigaku MiniFlex II instrument using Cu Kα radiation (λ = 1.54184 Å) at a scan rate of 0.3–0.6°/min to determine structure type and purity. Morphology and elemental composition were determined via scanning electron microscopy/energy dispersive spectroscopy (SEM/EDS) on a ZEISS 1550VP instrument equipped with an Oxford X-Max SDD energy dispersive X-ray spectrometer. Atomic ratios (atomic %) were reported as Si(M)/T-atom ratios, where T = Si(M) + Al + P and M is either Co or Mg, or Si(M)/(Al + P). To determine the micropore volume using the t-plot method (or the pore volume measured at P/P_0 = 0.01), N_2-

adsorption/desorption experiments were performed on selected samples at 77 K in a Quantachrome Autosorb iQ adsorption instrument using a constant-dose method. Prior to adsorption measurements, all samples were outgassed at 60 °C for 0.5 h, followed by holds of 0.5 h at 120 °C and 6 h at 350 °C (all ramping rates were 1 °C/min). Thermogravimetric analysis (TGA) measurements were performed on Perkin Elmer STA 6000. As-synthesized (prior to thermal treatment) or fully coked samples (0.02–0.06 g) were placed in an alumina crucible and heated at 7–10 °C/min in a flowing stream (0.33 cm^3/s) of air to 700–800 °C. Liquid ^{13}C NMR spectra were recorded on a Bruker 400 MHz spectrometer whereas liquid ^{1}H NMR spectra were recorded on a Varian INOVA 500 MHz spectrometer. All liquid NMR analyses, involving OSDAs, were performed in deuterium oxide (D_2O) (99.9 %, Cambridge Isotope Laboratories, Inc.).

All solid-state, magic-angle spinning nuclear magnetic resonance (MAS NMR) spectroscopy experiments were conducted on a Bruker Avance 500 MHz spectrometer using a 4 mm ZrO_2 rotor. The number of Brønsted acid sites was measured using quantitative ^{1}H MAS NMR spectroscopy. In a typical experiment, the thermally treated samples were dehydrated under vacuum (10^{-2} Torr) at 400 °C for 10 h at a ramp rate of 2 °C/min in a dehydration manifold after being pre-packed in an uncapped ZrO_2 rotor that is placed inside of a 5 mm glass NMR tube. The rotor was then capped while under vacuum and inside the dehydration manifold (to minimize sample exposure to moisture) and then loaded into the spectrometer. Spectra were collected at 500.20 MHz and a spinning rate of 12 kHz using a 90° pulse length of 4 μs. Recycle delay time was varied depending on the T_1 relaxation time of the samples. Signal intensities were referenced to hexamethylbenzene and normalized by the mass packed into the rotor for quantification. The spectra were deconvoluted using DMFit, as demonstrated in our previous work [27]. For ^{29}Si MAS NMR spectroscopy, oxygen was introduced to the dehydrated sample to reduce the relaxation time. The ^{1}H-decoupled ^{29}Si MAS NMR spectra were then acquired at 99.38 MHz and a spinning rate of 8 kHz using a 90° pulse length of 4 μs and a cycle delay time of 10 s. The acquired spectra were used to identify different Si environments in the tested samples. ^{27}Al MAS NMR spectra were acquired on the dehydrated samples (4 h at 400 °C at a ramp rate of 2 °C/min) at 130.2 MHz and at a spin rate of 13 kHz, a π/18 pulse length of 0.5 μs, and a cycle delay time of 0.5 s. ^{31}P MAS NMR spectra were also acquired on the dehydrated samples (4 h at 400 °C at a ramp rate of 2 °C/min) at 202.4 MHz at a spin rate of 12 kHz, a π/2 pulse length of 4 μs, and a cycle delay time of 4 s.

2.6. Catalytic testing

Catalyst evaluation was carried out in a fixed-bed reactor at ambient pressure. In a typical experiment, approximately 170–200 mg of dried catalyst (35–60 mesh size) was loaded between two layers of quartz wool in a 0.25″ × 6″ stainless steel (or quartz) tube reactor as a part of a BTRS Jr. continuous flow reactor (Parker Autoclave Engineers). The dry weight of the catalyst was estimated on the basis of thermogravimetric analysis (TGA; PerkinElmer STA 6000). All catalysts were first pretreated by heating to 150 °C at 1 °C/min, held for 3 h, and then heated further to 580 °C at 1 °C/min and held for 12 h under flowing air (breathing-grade D, AirGas). Methanol was introduced via a liquid syringe pump (Harvard Apparatus Pump 11 Elite) into a gas stream of an inert blend (95 % He and 5 % Ar; GC internal standard) at a volumetric flow rate of 30 cm^3/min. The methanol flow rate was adjusted, depending on the actual weight of the dried catalyst loaded in the reactor, to achieve a weight hourly space velocity (WHSV) of 0.65–2.6 h^{-1}. Reactions were performed at 300–450 °C. Effluent gases were evaluated using an on-stream Agilent GC–MS (GC 6890 N/MSD5793N) equipped with a Plot-Q capillary column. Aliquots of product flow were analyzed every ca. 16 min. All selectivity values were calculated on carbon-number basis.

In experiments where the content of the entrained hydrocarbons was of interest, the reaction was quenched rapidly (approximately −7 °C/s) after 5 min of reaction and a portion of the catalyst bed (20 mg) was transferred to a Teflon tube and suspended in 1.0 cm^3 of 48 % aqueous hydrofluoric acid (Sigma Aldrich). The solution was stirred for 2 h to allow the framework to dissolve. Following dissolution, the organic material was extracted into 1 cm^3 of dichloromethane (2 x 0.5 cm^3). Hexachloroethane (Aldrich, 99 %) was used as an internal standard. The speciation of aromatics in the organic layer was then identified using a mass spectrometer (Agilent 6890 N) and a ZB-5MS column (30 m x 0.25 mm) and quantified using a gas chromatograph (Agilent 7890B) connected to a Polyarc. The organic compounds extracted were identified in comparison with the NIST database as well as standards.

3. Results and discussion

3.1. Synthesis and characterization of CHA- and AEI-type materials

Among the various SAPO-type molecular sieves that have been tested in MTO, CHA and AEI-type materials have received the most attention in the MTO literature due to their outstanding catalytic performance, and in the case of SAPO-34 (CHA), its commercialization. Herein, we synthesized several CHA-, CHA/AEI-, and AEI-type molecular sieves (namely, SAPOs and MAPOs; M = Mg and Co) using various methods and OSDAs as outlined in the Experimental Section, for comparison against the SAT-type molecular sieves (discussed in the next section). The characterization data of these CHA- and AEI-type materials are provided in the Supplemental Information.

The PXRD patterns of the CHA, CHA/AEI, and AEI samples are shown in Figs. S3-S5. These patterns are in good agreement with simulated patterns (IZA database) as well as diffraction patterns reported previously for such materials [26,46,66]. The PXRD pattern of SAPO-34/18 (CHA/AEI) indicates that this sample is made up primarily of CHA and only has as a small amount of AEI. The MTO reaction behavior (*vide infra*) supports this conclusion. While we did not attempt to determine whether this sample is a true intergrowth or a physical mixture of CHA and AEI phases (the latter is a possibility), the PXRD pattern of the formed product, the uniform particle sizes of the sample (from SEM), and the choice of OSDA and gel composition employed in the synthesis (based on the literature) taken together suggest that this sample is likely an intergrowth that is comprised primarily of CHA.

The chemical compositions of the various CHA, CHA/AEI, and AEI samples were determined by EDS and these results are shown in Table S4. In this work, we synthesized an array of samples encompassing a broad range of Si(M)/T-atom ratios, where T = Si(M) + Al + P and M is either Mg or Co. However, because SAT typically crystallizes as a pure or near-pure product only when the Si or M content is low in the gel (discussed in more detail in the next section), the majority of the CHA- and AEI-type samples investigated and subsequently tested in MTO had Si(M)/T ratios in the range of 0.03 to 0.08.

Fig. S6 shows the SEM images of a select group of CHA and AEI samples. SEM images of samples not provided in Fig. S6 were reported in our previous work [18]. The SEM images show that the majority of the CHA, CHA/AEI and AEI samples have similar particle sizes (~0.5–3 μm). SAPO-34–3 and CoAPO-34 are the only two samples that have particle sizes that fall outside of this range. These materials have slightly larger particle sizes (~3–20 μm), likely because they were synthesized with morpholine as an OSDA. Morpholine has been associated with the production of CHA-type materials with relatively large particle sizes [68].

Due to the large number of CHA and AEI samples synthesized in this work, we designated SAPO-34–1, SAPO-34/18, and SAPO-18–1 as representative materials for each framework (or class of material) (i.e., CHA, CHA/AEI, and AEI). These materials were then further characterized using other techniques. Figs. S7-S9 show solid-state NMR results for these three samples.

The silicon distribution for these representative SAPO materials was investigated using solid-state ^{29}Si MAS NMR spectroscopy. SAPO

materials generally generate resonances ranging from approximately −91 to −112 ppm, corresponding to the presence of Si(4Al) (isolated Si atoms), Si(3Al), Si(2Al), Si(1Al) and Si(0Al) (Si islands). The ^{29}Si MAS NMR spectra for SAPO-34–1 (Fig. S7), SAPO-34/18 (Fig. S8), and SAPO-18–1 (Fig. S9) demonstrate that all samples have a main resonance in the range of −95.4 to −95.6 ppm, with the SAPO-34–1 sample showing a slightly more diverse set of Si environments than the other samples. However, all of the CHA, CHA/AEI and AEI representative samples are made up of mostly Si(4Al) and Si(3Al) environments, likely due to the low Si content in these materials. SAPO-18–1 has a very weak signal as a result of it having the lowest Si content of all the samples.

Additionally, ^{27}Al and ^{31}P solid-state NMR experiments were performed on the three representative materials. The CHA (SAPO-34–1) and CHA/AEI (SAPO-34/18) materials have a strong resonance in the ^{27}Al MAS NMR spectra at approximately 35 ppm, which corresponds to tetrahedrally coordinated Al. The SAPO-18–1 sample shows a main resonance centered at 34.5 ppm (similar to what has been observed on AlPO-18 materials previously) [69], which corresponds to tetrahedrally coordinated Al, and a small peak at approximately 9 ppm, which is assigned to penta-coordinated Al species. Furthermore, the ^{31}P MAS NMR experiments demonstrate that all the samples had a single resonance at approximately −30/-31 ppm, which is consistent with tetrahedrally connected AlPO-18(34)/SAPO-18(34)-type materials.

To investigate the acidity of the catalysts and measure their acid site densities, ^{1}H NMR experiments were performed on the dehydrated samples (SAPO-34–1, SAPO-34/18, and SAPO-18–1) and the obtained spectra are shown in Figs S7-S9. Two main peaks were observed, which are consistent with two differently formed acid sites: a weaker acid site showing a dominant resonance at ca. 3.6–3.7 ppm and a stronger acid site showing a resonance at 3.9–4 ppm. Deconvolution of these peaks gives rise to the total acid site density values measured for these three samples. SAPO-34–1, SAPO-34/18, and SAPO-18–1 have Brønsted acid site densities of 1.09, 0.89, and 0.68 mmol/g, respectively.

N_2-adosprtion-desorption experiments were also performed on the three representative CHA, CHA/AEI, and AEI samples, and the obtained micropore volumes (V_{micro}) were 0.24, 0.25, and 0.18 cm^3/g for SAPO-34–1, SAPO-34/18, and SAPO-18–1, respectively.

3.2. Synthesis and characterization of SAT-type molecular sieves

MgAPO-SAT- and CoAPO-SAT-type molecular sieves were initially synthesized based on previously reported methods and gel compositions. We then examined the formation of these products over a slightly wider range of synthesis conditions (listed in the Supplemental Information) and discussed in the Experimental Section. STA-2-type materials (e.g., MgAPO-SAT) have been previously characterized in the literature rather thoroughly [55–57]. As such, for brevity, in this work, we only confirm the formation of these two products (MgAPO and CoAPO) by PXRD and measure each sample's elemental composition by EDS. Interested readers are referred to the original STA-2 work, which contains numerous characterization data on SAT-type metalloaluminophosphates.

Fig. S10 shows the PXRD patterns of MgAPO-SAT as well as CoAPO-SAT, which are in agreement with the previously published patterns for STA-2. The elemental composition data show that MgAPO-SAT and CoAPO-SAT have a M/T-atom ratio of 0.071 and 0.063, respectively, as shown in Table S4.

As indicated earlier, SAT was first discovered in 1997 as a MgAPO (STA-2) using DiQ-C_4 as an OSDA [55]. The following gel led to the formation of STA-2 (MgAPO), albeit the formed product, as reported by the authors, contained some amorphous phases (evidenced by PXRD, SEM, and the reported void volume of 0.095 cm^3/g): 0.45 Al_2O_3: 0.5 P_2O_5: 0.1 Mg: 0.4 $R(OH)_2$ (R = DiQ-C_4): 40 H_2O [55]. As a part of that early work on STA-2, the authors showed that increasing the Mg/P ratio (to 0.15 in the gel) led to the co-crystallization of MgAPO-56 (AFX), whereas in another set of experiments, they demonstrated that substituting $R(OH)_2$ for $R(Br)_2$ and sodium hydroxide (as the source of OH^-) led to formation of AFX as well. These experimental results demonstrate the ability of DiQ-C_4 to structure direct both AFX and SAT. However, the gel composition appears to play a significant role in steering the product toward one of these structures.

In 2010, in a follow-up experimental and theoretical study [56], the authors showed that DiQ-C_4 could be substituted for a less expensive molecule, DiDABCO-C_4, and still form STA-2 [56]. In total, the authors proposed and examined three OSDAs that could template STA-2 ($AlPO_4$, MgAPO and SAPO): DiQ-C_4, DiDABCO-C_4, and DiDABCO-C_5. Slight changes were applied to the Al/P ratio in the new proposed gel (in comparison to the original gel proposed in the 1997 work), but otherwise, the OSDA concentration in the hydroxide form remained elevated (0.4–0.5) in all trials. In this work, the authors were able to obtain $AlPO_4$-SAT as a pure product and more importantly, synthesize SAT using a much more affordable molecule. However, attempts to synthesize SAPO-SAT persistently led to the co-crystallization of SAPO-56 (AFX) with SAT.

To the best of our knowledge, it does not appear that SAPO-SAT has been crystallized in a pure form since the discovery of the first SAT material (STA-2; MgAPO-SAT) almost two decades ago. Recently, as a part of a program to synthesize small-pore, cage-type molecular sieves, we encountered a disordered phase, which we denoted as CIT-16P. CIT-16P, which is synthesized using DiQ-C_4, was found to have a relatively similar structure to a recently reported zeotype material denoted as ECNU-38P (although each material is synthesized with a different OSDA and gel composition) [70]. We showed that CIT-16P crystallizes in a gel that is not too far from STA-2, but only when the OSDA (DiQ-C_4) concentration was lower than 0.28. In our CIT-16P work, SAT appeared often as an impurity phase when the OSDA concentration was higher than 0.28 in the gel or lower than 0.24. AFX was the other impurity phase appearing in that work (often when the Si content was high).

Following the discovery of CIT-16P and realizing that SAPO-SAT has not been synthesized in a pure form yet (i.e., in the absence of SAPO-56), we hypothesized that the hydroxide ion content in the gel might be the differentiating factor that could lead to the formation of SAPO-SAT without AFX. Tables S1-S3 list the gel compositions that were attempted to synthesize various SAT-type molecular sieves with different OSDAs (DiQ-C_4 in Table S1, DiQ-C_5 in Table S2, and DiDABCO-C_4 in Table S3). Pure SAPO-SAT was denoted as CIT-17.

Our experimental results on the synthesis of CIT-17 demonstrate the importance of regulating the hydroxide content in the gel by keeping the OSDA content between 0.17 and 0.22 (when H_2O is 40), particularly when DiQ-C_4 and DiDABCO-C_4 are used as OSDAs. Since CIT-16P does not form when using the longer OSDA (DiQ-C_5), the gel becomes more tolerant of the hydroxide content coming from the DiQ-C_5 OSDA (up to 0.27) while still leading to the formation of CIT-17. Our results show that the key factor to forming SAT is not necessarily the total amount or type of R^+ that is added to gel (there is quite a bit of flexibility when it comes to these two parameters), but rather the hydroxide amount/concentration that is accompanying that OSDA (see Entries 20–22 and Entries 42 to 49 in Tables S1-S3). For instance, one can increase the OSDA content, but also increase the water content simultaneously and still make CIT-17 (because in doing so, the changes in pH are mitigated). Or, one can add the ideal amount of OSDA (in the hydroxide form) then add more OSDA in the bromide form and still make CIT-17.

Our experimental results also show that there is some flexibility in terms of changing the Al/P ratio in the gel while still making a relatively pure or near-pure CIT-17 product. Furthermore, our results demonstrate that CIT-17 can be prepared under rotating or static conditions. Of all the parameters tested, Si was one parameter (in addition to the hydroxide concentration) that appears to influence the purity of CIT-17 rather significantly, especially in terms of eliminating the AFX phase (SAPO-56). For the majority of our experiments, we observed that once the Si content is increased above 0.1 in the gel, impurity phases appear and the peaks associated with AFX continue to increase as the Si content

is further increased (see Entry 50 in Table S3).

Figs. S11-S12 show the PXRD patterns of a select group of CIT-17 samples. Minor shifts in the diffraction peaks are observed among the various SAT samples, likely owing to small differences in unit cell size caused by differences in composition and choice of OSDA in the synthesis procedure. Fig. S13 shows the SEM images of all the CIT-17 samples that are later tested in the MTO reaction. All the samples had particles that were comparable in size (~0.3–4 μm) and morphology (i.e., rhombohedral), irrespective of which OSDA was used during synthesis. However, the DiDABCO-C_4 OSDA (CIT-17–3) did form particles that were on the lower end of this range (~0.3–1 μm). Additionally, the sample that had higher Si content (CIT-17–5) contained more amorphous-like phases and a small amount of AFX impurities. AFX (SAPO-56) has a distinct hexagonal plate-like or disk-like morphology, as reported previously [71]. Particles with AFX-like morphologies were observed in the SEM images of CIT-17–5, in agreement with the PXRD patterns.

Due to the large number of CIT-17 samples synthesized in this work, we selected CIT-17–4 as a representative CIT-17 sample for further characterization. Fig. 2a shows the PXRD pattern of the as-synthesized CIT-17–4 material, which agrees with previously published patterns for STA-2. Fig. 2b shows an SEM image of the as-synthesized form of CIT-17–4, revealing that it has particle sizes of ca. 0.5–2 μm.

TGA shows that the corresponding mass loss due to the OSDA (DiQ-C_5) removal from heating in air (calculated from the mass losses between 300 and 800 °C) was approximately 17.6 % (Fig. 2c). For CIT-17–4, the major weight loss starts at approximately 380 °C, with the largest loss occurring near 500 °C due to the removal of the OSDA. We also performed TGA experiments (not shown) on two other samples that were synthesized using DiQ-C_4 (CIT-17–2) and DiDABCO-C_4 (CIT-17–3), and these materials had mass losses of approximately 18.1 % and 16.4 %. These values are in close accord with the value reported previously for STA-2 (ca. 17 %) [56].

^{13}C solid-state NMR on the as-synthesized CIT-17–4 sample was compared to the liquid ^{13}C NMR of DiQ-C_5, which shows that the OSDA was well preserved in the as-synthesized material following crystallization (Fig. 2d). ^{1}H MAS NMR was performed on the thermally treated CIT-17–4 sample following dehydration as outlined in the Experimental Section (Fig. 2e). Similar to the CHA and AEI materials discussed previously, two major resonances are detected: one at ca. 3.7 ppm and the other at 4 ppm. The broad resonances from 1 to 3 ppm are likely due to P-OH (at approximately 2.6 ppm) and Si-OH (at approximately 1.8 ppm) [72]. The Brønsted acid site density of this sample was calculated to be 0.28 mmol/g (based on the 3.7 and 4 ppm peaks). ^{29}Si MAS NMR shows a mixture of Si environments, with a clear resonance at approximately −96.5 ppm (Fig. 2f). This is consistent with the presence of various Si

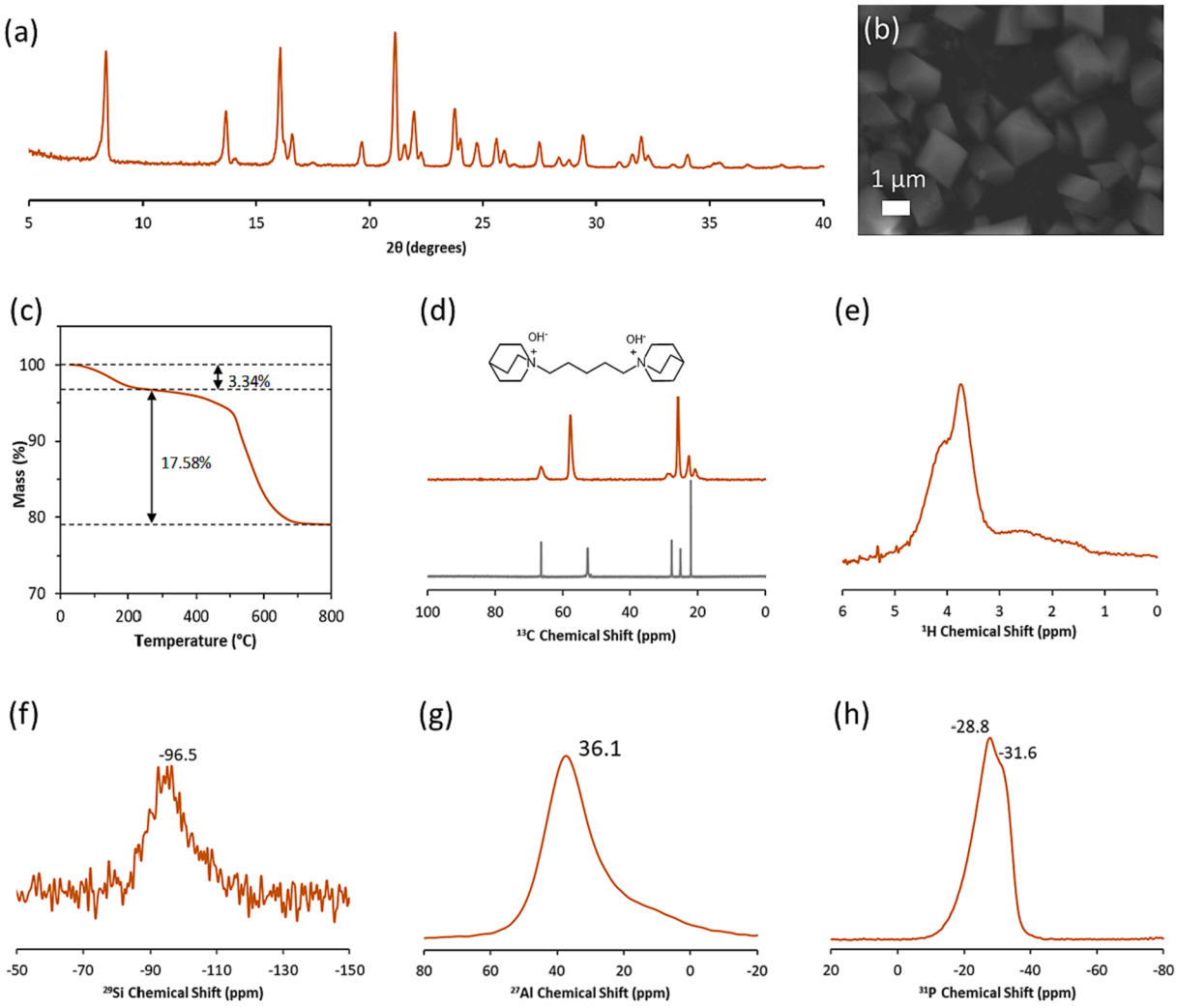

Fig. 2. Characterization data of CIT-17-4. (a) PXRD pattern of the as-synthesized sample. (b) SEM image of the as-synthesized sample. (c) TGA profile of the as-synthesized sample. (d) solid-state ^{13}C NMR of the as-synthesized sample (top) compared to the liquid (bottom) ^{13}C NMR spectrum (DiQ-C_5). (e) ^{1}H MAS NMR spectrum on the thermally treated sample (after dehydration). (f) ^{29}Si MAS NMR spectrum of the thermally treated sample (dehydrated then treated with oxygen). (g) ^{27}Al MAS NMR spectrum of the thermally treated sample (dehydrated). (h) ^{31}P MAS NMR spectrum of the thermally treated sample (dehydrated).

environments as described previously for CHA and AEI. ^{27}Al MAS NMR shows one broad resonance centered at 36.1 ppm whereas ^{31}P MAS NMR shows two overlapping resonances at −28.8 and −31.6 ppm (Fig. 2g and Fig. 2h). It was previously reported by Castro et al. [56] that SAT $AlPO_4$-type materials have two distinct Al resonances (as determined via ^{27}Al MAS NMR) and two distinct P resonances (as determined via ^{31}P MAS NMR) due to the structure of the SAT framework, which is built up of layers of CAN cages in which these cages share 4MRs (Fig. S1). These layers are attached to D6Rs, which are connected to the large SAT cage. One type of the Al and P set is located in the 4MRs whereas the other set is located in the planar 6MRs of the CAN cages [56].

Using N_2-physisorption, a pore volume was calculated for this sample (0.18 cm^3/g at $P/P_0 = 0.01$). As mentioned earlier, MgAPO-SAT (STA-2) was reported to have a void volume of 0.095 cm^3/g, although this was a sample that contained some amorphous phases [55].

3.3. MTO reaction testing

The reaction results for the various CHA-, CHA/AEI-, AEI-, and SAT-type molecular sieves that were characterized in the previous sections are summarized in Table 1. Fig. 3 shows the averaged propylene-to-ethylene ratio of the evaluated catalysts (when methanol conversion is greater than 97 %) for the three main framework types investigated. The time-on-stream (TOS) reaction profiles are provided in the Supplemental Information (Figs. S14-S19).

To establish a benchmark for the product distribution analysis, several CHA-type molecular sieves with varying elemental compositions and Si(M)/T-atom ratios were tested at identical reaction conditions (temperature (T) = 400 °C and WHSV of 1.3 h^{-1}). The SAPO-CHA-type materials (SAPO-34-series) showed results that were consistent with the literature data. The SAPO-34 samples, irrespective of Si/T ratio, exhibited high relative stability, low alkane products, and high combined ethylene (28–31 %) and propylene (38–41 %) selectivities. These ethylene and propylene selectivities correspond to P/E ratios of approximately 1.3 for all three SAPO-34 samples tested (SAPO-34–1, SAPO-34–2, and SAPO-34–3). The three SAPO-34 samples also produced a relatively low C_{4+} fraction. SAPO-34/18, which as mentioned earlier, is made up mostly of CHA (based on the PXRD), also behaved similarly to the SAPO-34 samples tested in this work, giving off a P/E of 1.31 (Table 1). These results on SAPO-34 are consistent with the findings of Peng and co-workers [43], as the authors observed that changing the Si/T-atom ratio (i.e., acid site density) effects mainly catalyst deactivation and to a much lesser degree the light olefins selectivities.

Metal-substituted $AlPO_4$'s (MAPOs) are a class of molecular sieves that have been tested in the MTO reaction, albeit they have received less attention in the MTO literature than SAPOs and zeolites (aluminosilicates). The substitution of different heteroatoms into the $AlPO_4$ structure affects the Brønsted acid site strength of the catalyst, thus, leading to differences in the catalytic performance, as has been demonstrated previously [31].

Two MAPO-34 (M = Mg or Co) samples that were denotated as MgAPO-34 and CoAPO-34 were tested. The reaction data from these two samples show that substituting Si for Mg or Co (as the method for creating the acid site) in the $AlPO_4$ structure results in a slight reduction in the P/E ratio (from 1.3 for the SAPO-34-series samples down to 0.91–0.97 for the MAPO-34 samples). A closer look at the data in Table 1 shows that each of these two catalysts enhances primarily the ethylene selectivity. We have reported previously on this behavior [18]. The degree in improvement in the ethylene-to-propylene ratio (E/P) observed in the MAPO-34 materials is similar to the enhancement in the E/P ratio that we observed and reported on when testing various SSZ-13-type materials in MTO, a zeolite that is isostructural to SAPO-34. As we demonstrated in that work, the slight improvement in the E/P ratio exhibited by the various SSZ-13 samples, which had Si/Al ratios ranging from ca. 5 to 55, and the deviation in the catalytic performance of SSZ-13-type materials from SAPO-34 (in terms of alkane selectivities and lifetime) were due to differences in acidity (i.e., Brønsted acid site density, proximity, and strength) [26].

While there are only a few reports on the use of MAPO materials in the MTO reaction, the insertion of Mg or Co into an $AlPO_4$-based structure results in the formation of acid sites that have different strengths (typically, stronger) than the sites generated by Si substitution [31]. As such, the olefins product distribution differences observed in this work between the MAPO-34 samples and the SAPO-34-series samples are likely due to differences in acid site strength. Nevertheless, all the CHA-type materials tested here, irrespective of composition, give a propylene-to-ethylene ratio in the range of 1 to 1.3 (Fig. 3).

AEI is another framework that has received considerable interest in the MTO literature due to its ability to enhance the P/E ratio when compared to other small-pore, cage-type molecular sieves. Previously,

Table 1
Reaction results of the SAPO materials investigated. (Note: multiply selectivity values by 100 to convert them to percentages).

Parameter	Framework	Material ID	Si(M)/T	Temperature (°C)	WHSV (h^{-1})	Averaged Selectivities (at 97–100 % Conversion)					
						$C_{2=}$	$C_{3=}$	$C_2 + C_3$ Alkanes	C_4	C_{5+}	$C_{3=}/C_{2=}$
Effect of Cage Size	**CHA**	**SAPO-34-1**	0.081	400	1.3	0.31	0.41	0.048	0.10	0.05	1.31
		SAPO-34-2	0.123	400	1.3	0.30	0.39	0.053	0.13	0.07	1.30
		SAPO-34-3	0.127	400	1.3	0.28	0.38	0.091	0.12	0.04	1.35
		MgAPO-34	0.015	400	1.3	0.41	0.40	0.034	0.10	0.04	0.97
		CoAPO-34	0.022	400	1.3	0.44	0.40	0.029	0.09	0.04	0.91
	CHA/AEI	**SAPO-34/18**	0.063	400	1.3	0.31	0.40	0.050	0.09	0.05	1.31
	AEI	**SAPO-18-1**	0.038	400	1.3	0.23	0.48	0.067	0.16	0.08	2.10
		SAPO-18-2	0.061	400	1.3	0.22	0.47	0.081	0.15	0.09	2.13
		SAPO-18-3	0.162	400	1.3	0.20	0.43	0.092	0.18	0.12	2.19
		MgAPO-18	0.031	400	1.3	0.17	0.40	0.134	0.19	0.09	2.34
		CoAPO-18	0.073	400	1.3	0.19	0.42	0.110	0.19	0.14	2.17
	SAT	**CIT-17-1**	0.068	400	1.3	0.14	0.48	0.031	0.17	0.15	3.40
		CIT-17-2	0.072	400	1.3	0.13	0.47	0.021	0.17	0.15	3.62
		CIT-17-3	0.073	400	1.3	0.15	0.47	0.038	0.16	0.13	3.23
		CIT-17-4	0.083	400	1.3	0.16	0.49	0.037	0.17	0.13	3.15
		CIT-17-5	0.094	400	1.3	0.19	0.47	0.047	0.16	0.12	2.47
		MgAPO-SAT	0.071	400	1.3	0.18	0.35	0.080	0.16	0.15	2.01
		CoAPO-SAT	0.063	400	1.3	0.18	0.42	0.063	0.16	0.13	2.33
Effect of Reaction Conditions	**SAT**	**CIT-17-4**	0.083	450	0.65	0.28	0.46	0.031	0.11	0.08	1.64
		CIT-17-4	0.083	400	0.65	0.18	0.40	0.033	0.17	0.09	2.22
		CIT-17-4	0.083	400	2.6	0.14	0.49	0.047	0.15	0.15	3.50
		CIT-17-4	0.083	350	1.3	0.12	0.45	0.050	0.19	0.18	3.75
		CIT-17-4	0.083	350	0.65	0.12	0.50	0.034	0.20	0.12	4.17

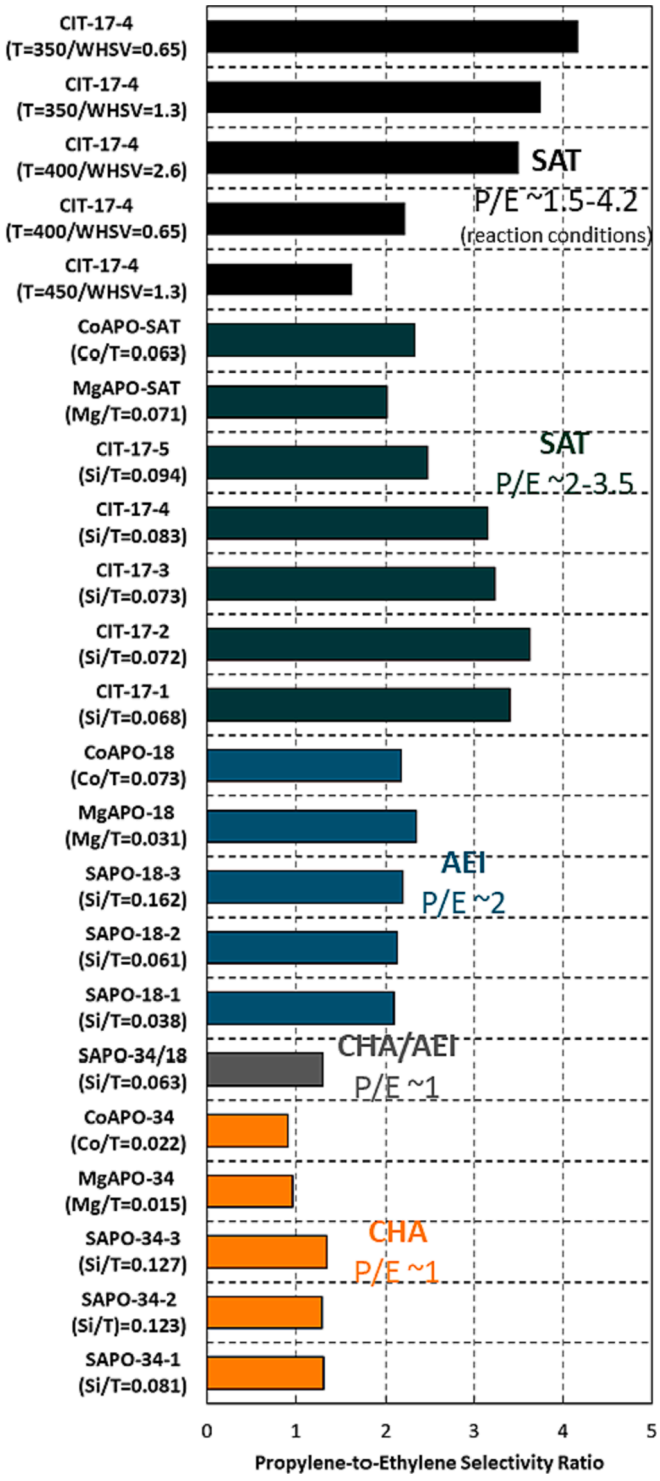

Fig. 3. Averaged propylene-to-ethylene (P/E) ratios of the various materials investigated in this work at complete or near-complete methanol conversion (97+%).

we showed that both SAPO-18 (AEI) and SSZ-39 (AEI), the zeolitic analogue, are able to enhance the propylene selectivity over CHA-type materials [18,28]. In fact, of the 14 different small-pore, cage type frameworks that we previously tested in MTO, AEI was found to give one of the highest P/E ratios combined with the lowest C_{4+} fractions [18].

Since the AEI topology significantly improves the propylene selectivity over CHA-type materials, several SAPO-18 (AEI) samples, with different Si/T-atom ratios, were tested for comparison. Fig. S16 shows the time-on-stream reaction data for the various AEI samples tested. Similar to our observations on SAPO-34 catalysts, all three of the SAPO-18 samples (SAPO-18–1, SAPO-18–2 and SAPO-18–3) had comparable P/E ratios (ca. 2). While the effect of changing the Si/T-atom ratio (thus, acidity) on the olefins product distribution was similar across the CHA- and AEI-SAPO-type materials, showing little to no effect, the effect of changing the cage size, in going from the smaller CHA cage (CDR = 7.45 Å) to the larger AEI cage (CDR = 8.52 Å) is far more signficant, and results in an enhancement in the propylene selectivity. These improvements are reflected in the elevated P/E ratios reported in Table 1 and shown in Fig. 3.

In addition to the SAPO-18-series samples, two AEI-type MAPOs were also investigated: MgAPO-18 and CoAPO-18. The data show that changing the elemental composition (and hence acidity) of AEI-type molecular sieves does not result in significant changes in the light olefins selectivities. We did however observe that the MAPO-18 catalysts generally deactivated faster (i.e., shorter lifetimes) than the SAPO-18 catalysts (also the case with the CHA-type MAPOs when compared to SAPO-34).

The observations on CHA- and AEI-type matarials are consistent with what has been reported in the literature. The effect of cage size is more significant in influencing the olefins product distrubition in MTO than the effect of Brønsted acidity, with larger cages such as AEI forming more propylene and butenes than CHA. However, we also showed previously that by opting for cages larger than AEI (e.g., KFI, LTA and RHO), the olefins product disturbution starts to shift to favor more butenes formation, which hold less value industrially than propylene [18,53]. Since changing the acidity (both acid site strength and distrubtion) of both CHA and AEI-type molecular sieves does not appear to *considerbly* enhance the P/E ratio (in agreement with several prior studies) [22,43,66], we attempted to improve the P/E ratio by investigating SAT-type molecular sieves in the MTO reaction.

The SAT framework has one of the narrowest cages (CDR size = 6.6 Å) that can accommodate aromatic-type hydrocarbon pool species in the MTO reaction. We originally planned to test SAT-type molecular sieves in this reaction to improve the ethylene selectivity because: (i) the product distribution trends that we previously observed in our cage-defining ring size work (i.e., small cages with smaller CDRs lead to the formation of lighter olefins) and (ii) the structural parameter, $E_{int(7/5)}$, relationships that were proposed by Ferri and co-workers, which correlate the degree of methylation of the entrapped methylbenzenium cations and the MTO product distribution selectivity to ethylene, propylene and butenes [18,22] both suggested that the smaller cage size would favor ethylene. However, by selecting a framework with a relatively narrow cage such as SAT, which is narrower than ERI (has a CDR size of 6.75 Å), we might also observe similar trends as the ones we uncovered in our previous work on ERI-type molecular sieves (mentioned in the introduction), where the catalyst acidity contributed to the observed olefins product distribution in tandem with cage size. Indeed, we previously demonstrated that that ERI cage can improve the E/P in the MTO reaction only when the Si/Al ratio was low in zeolites (Si/Al < 7; thus, higher acid site density) or the Si/T-atom ratio was high in the SAPOs (Si/T > 0.1) [27]. These effects were unique to ERI and was not something that we observed in CHA, AEI, AFX, and several other frameworks [18,20]. Results from dissolution-extraction experiments shed light on why ERI behaves so differently. ERI, likely due to its narrow cage, accumulates aromatic HP species at a much slower rate than CHA-type molecular sieves (SSZ-13 and SAPO-34). By increasing the Si/T ratio or lowering the Si/Al ratio, the ERI samples are able to accumulate aromatics at a much faster rate. These aromatic species are comprised of partially methylated benzenes (1–4 MB) as well as naphthalenes, which are species that are associated with the aromatics cycle. Thus, we concluded that the slower maturation of aromatics species coupled with the high $C_{4+}/C_{2=}$ ratios detected early in the reaction are likely indicative of a higher contribution from the olefins cycle.

Since SAT materials can only be synthesized over a narrow Si(M)/T

range where the Si or M content in generally low, we hypothesized that we may be able to design a catalyst that would take advantage of the narrow structural features of SAT and the low acid-density (i.e., low Si (M)/T) of currently available SAT materials (e.g., STA-2 and CIT-17) to improve the P/E ratio in the MTO reaction. Table 1 shows the MTO olefins product distribution of several SAT-type molecular sieves, including the various CIT-17 samples. Fig. 3 shows data that reveal that all the CIT-17 catalysts gave improved P/E ratios over SAPO-34 (CHA), although the degree of enhancement was a strong function of Si/T ratio. Indeed, our results demonstrate that lowering the Si/T ratio leads to higher P/E ratios (2–3.62). These data are consistent with the behavior and trends observed in our previous ERI work. Additionally, the reaction data shown in Table 1 reveal that there are no considerable differences between the olefins product distribution of the various CIT-17 samples with comparable Si/T ratios (even though they are synthesized with different OSDAs; CIT-17–1, CIT-17–2 and CIT-17–3).

When comparing the MTO behavior of the SAT-type molecular sieves to those of CHA and AEI, two differences standout: lifetime and product distribution. The TOS data for the CIT-17 samples show that they exhibit shorter lifetimes than the SAPO-34 and SAPO-18 samples investigated. This effect is likely due to the size of the SAT cage which is significantly narrower and longer than CHA and AEI cages, but should not viewed negatively as the commercial process is operated in a fluidized bed reactor, where rapid catalyst deactivation can be mitigated. In terms of product distribution, the reaction data in Table 1 show that the CIT-17 samples generate a higher C_{4+} fraction (ca. 31 %) than CHA (15 %) and AEI (25 %). This high C_{4+} fraction is not consistent with the cage size of SAT (one would expect a high ethylene selectivity and low butenes selectivities) but is likely an indication of a possible contribution from the olefins cycle (similar to the ERI case discussed previously) due to the low Si/T ratio of the samples. CIT-17 also accumulates less coke upon deactivating (discussed further in a subsequent section).

In addition to studying the SAPO-SAT (CIT-17) samples, we tested two MAPO-SAT materials, MgAPO-SAT and CoAPO-SAT. These materials gave lower P/E ratios (i.e., higher E/P ratios) than CIT-17 (P/E = 2.1–2.33 compared to P/E = 2.47–3.6 for CIT-17), consistent with the catalytic behavior of other MAPO materials investigated in this work (i.e., they mainly enhanced the ethylene selectivity). Even though the MAPO-SAT samples had lower P/E ratios than CIT-17, they still gave P/E ratios that were higher than CHA. Furthermore, a closer look at the data in Table 1 show that inserting Mg or Co (instead of Si) in $AlPO_4$-structures results in an improvement in the ethylene selectivity and a reduction in the propylene selectivity in SAT-type molecular sieves. This improvement in the E/P ratio (and ethylene selectivity) is more significant in the case of MAPO-SAT than in the case of MAPO-34 and MAPO-18 (MAPO-SAT > MAPO-34 > MAPO-18).

3.4. Changing the reaction conditions to further enhance the P/E with SAT

All the reactions in the previous section were conducted at identical reaction conditions (400 °C and WHSV of 1.3 h^{-1}), to allow for comparisons between the various frameworks (cage size) and Si(M)/T ratios (thus, indirectly acidity). In this section, results from changing the reaction temperature (from 300 °C to 450 °C at 50 °C increments) and WHSV (0.65 to 2.6 h^{-1}) on the P/E ratio of CIT-17–4 are described.

Table 1 lists the reaction results from experiments where the reaction conditions were varied, and Fig. 3 shows the averaged P/E ratios. Fig. S19 shows the TOS data for these set of experiments. The data reveal that changing the reaction conditions has a profound effect not only on the olefins product distribution but also lifetime, in agreement with prior reports [33–35]. While high temperatures aid in improving the ethylene selectivity, lower temperatures result in faster deactivations. Also, lowering the reaction temperature down to 300 °C led to the formation of DME only (data not shown). Furthermore, from our experiments we found that it was necessary to lower the WHSV in order to better regulate and delay the catalyst deactivation (Fig. 3). Lowering the WHSV has been previously shown to alter the composition of HP species, steering them toward partially methylated benzenes which are associated with ethylene [33].

The MTO results obtained from varying the reaction conditions suggest that T = 350 °C and WHSV of 0.65 h^{-1} are near-optimal reaction conditions because they enhance the propylene selectivity over CIT-17 but do not significantly increase the ethylene selectivity (i.e., maintain a high P/E ratio) or compromise the catalyst lifetime. Fig. 4 shows the TOS data for CIT-17–4 at these reaction conditions. At these conditions, we were able to obtain averaged ethylene and propylene selectivities of approximately 12 % and 50 % at complete or near complete methanol conversion, resulting in a P/E ratio of approximately 4.17. This value is two times higher than that obtained from AEI and four times higher than that from CHA-type molecular sieves. This P/E ratio is, indeed, one of the highest P/E ratios achieved for this class of materials.

3.5. Relationships between effluent product and retained hydrocarbons

To rationalize the differences observed in the olefins product distribution and overall MTO behavior between the CHA, AEI, and SAT frameworks, dissolution-extraction experiments were performed on five samples exposed to identical reaction conditions (400 °C and WHSV of 1.3 h^{-1}): SAPO-18–1, SAPO-18–2, SAPO-34–1, SAPO-34/18, and CIT-17–4. These samples were chosen to represent one CHA, one CHA/AEI (although as mentioned earlier, this sample is mostly CHA), and two AEI materials with different Si/T atom ratios. These four samples were compared to CIT-17–4, one of the best performing SAT catalysts. For this analysis, each of these catalysts was reacted with methanol and the reaction stopped after 5 min to avoid the deactivating region of the reaction and rather focus on the early stage of reaction that is associated with the propylene enhancement effect. The reactor was then rapidly cooled to ambient conditions as described in the Experimental Section.

Fig. 5 shows the extracted hydrocarbons distribution for these five catalysts. Each of these catalysts contained primarily polymethylbenzenes (PMB) species. Of the total HP species recovered via this technique, 94+ mol% were polymethylbenzenes, with only a small amount of naphthalenes (<3 mol%) or alkylbenzenes (approximately 1 mol%) detected. The SAPO-34 and SAPO-34/18 samples accumulated primarily of tetra-, penta-, and hexamethylbenzenes (4 MB, 5 MB, and 6 MB). Both catalysts had similar PMB distributions, with the SAPO-34/18 sample showing a slightly lower relative concentration, likely due to the lower Si/T ratio (thus, acid site density) of this sample.

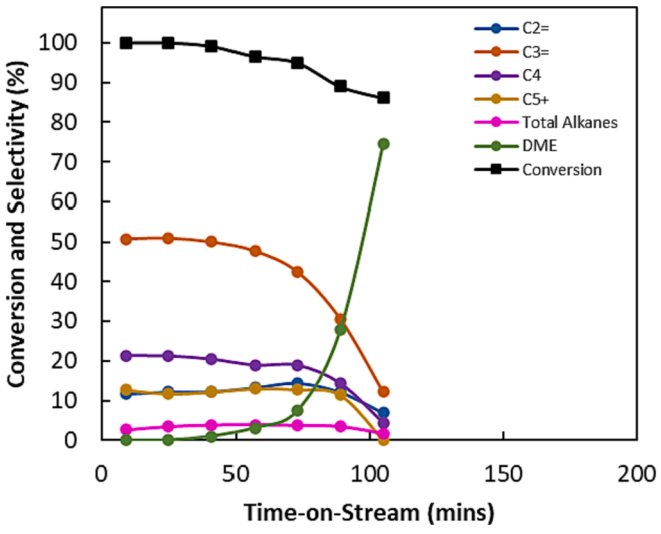

Fig. 4. Representative MTO reaction data obtained at 350 °C and WHSV 0.65 h^{-1} for CIT-17–4.

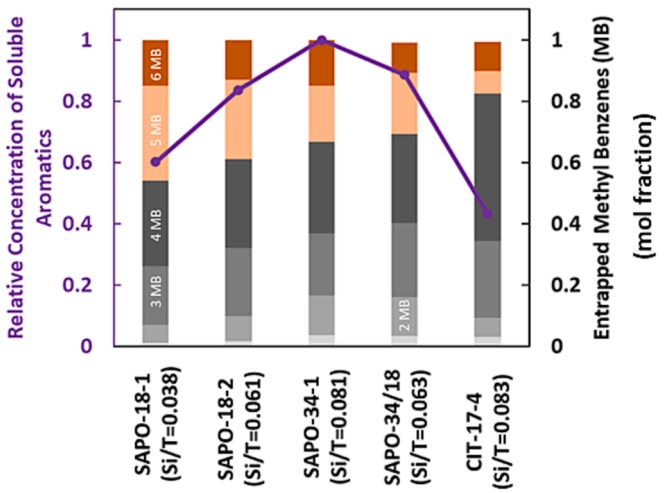

Fig. 5. GC–MS distribution of the extracted polymethylbenzene-type hydrocarbon species after five minutes of reaction with methanol at 400 °C and WHSV of 1.3 h^{-1} and their relative concentration (relative to SAPO-34-1).

Both SAPO-18 samples had much higher concentrations of 5 MB and 6 MB species than the SAPO-34 samples, in agreement with prior results and the notion that AEI-type molecular sieves improve the propylene selectivity over CHA-type material due to their ability to better accommodate higher substituted methyl benzenes [21,22,33]. Indeed, both frameworks (CHA and AEI) are known to proceed via the aromatics cycle, with the differences in their product distribution attributed to the type of entrapped species that form in both of these frameworks during reaction. Furthermore, the results shown in Fig. 5 reveal that SAPO-18–1 had a much lower concentration of aromatics than SAPO-18–2. This effect is likely due to the lower Si/T ratio, which also manifests itself in the TOS reaction data (the catalyst does not immediately achieve 100 % methanol conversion) (Fig. S16).

CIT-17–4 showed a high content of tri- and tetra-methylbenzenes (3 MB and 4 MB), which is consistent with the size of the SAT cage. However, this sample gave a high propylene selectivity in the beginning of this reaction (as opposed to high ethylene selectivity). Partially methylated benzenes such as, 3 MB and 4 MB, are typically associated with ethylene formation whereas 5 MB and 6 MB are associated with propylene formation [21,40,41]. Therefore, we measured the concentration of the soluble aromatics in this sample, which revealed that after identical reaction times with methanol (5 mins), CIT-17–4 accumulated about half the amount of aromatic species that SAPO-34–1 accumulated under similar conditions. Virtually all the CIT-17 samples tested in this work had high C_{4+} selectivities and a low ethylene selectivity (particularly early in the reaction). This, as in the case of ERI (discussed previously), suggests a contribution from the olefins cycle in SAT-type molecular sieves. Therefore, our data indicate that the high propylene selectivity (and low ethylene selectivity) exhibited by CIT-17 are the result of a much higher contribution from the olefins cycle whereas the high propylene observed in AEI-type materials are the result of changes in the identity of the entrapped HP species (i.e., more 5 MB and 6 MB). Thus, the enhancement in propylene selectivity observed in AEI-type and SAT-type materials over CHA-type molecular sieves appear to be mechanistically different.

3.6. Cyclic testing with CIT-17

Due to the ability of CIT-17-4 to enhance the propylene selectivity in the MTO reaction over CHA- and AEI-type molecular sieves, this catalyst was reused for six consecutive MTO reactions (Fig. 6). Without searching for an optimal catalyst regeneration strategy, a simple intermittent dry calcination in air was used (at 580 °C for 8 h at a ramp rate of 1 °C per minute). The results show that after each regeneration, we are able obtain a behavior and selectivities that are similar to the first run. Over six runs, the catalyst has efficiently converted methanol for about 10 h on stream at 350 °C. TGA was performed on the coked sample (after the sixth run) revealing that the material had a mass loss of 6.36 %, which is lower than the coke content that is typically recovered from CHA- and AEI-type materials (ca. 10–20 %) [27,28].

4. Conclusion

SAT-type molecular sieves (SAPO, MgAPO, and CoAPO) were synthesized using a number of OSDAs to form materials with different Si/T-atom ratios. The synthesis of CIT-17 (a SAPO-SAT material) was achieved without AFX impurities for the first time. These SAT materials were characterized using a myriad of techniques and tested as catalysts in the MTO reaction. The olefins product distribution of SAT-type molecular sieves was compared to CHA- and AEI-type materials. Both SAPO-18 (AEI) and CIT-17 gave improved propylene selectivities (i.e., improved P/E ratios) over SAPO-34 (CHA). Specifically, SAPO-18 gave a P/E ratio of approximately 2 whereas CIT-17 gave a P/E of 2 to 3.5. Changing the Si(M)/T ratio did not significantly enhance the olefins product distribution of CHA and AEI-type molecular sieves but did so in the case of SAT-type molecular sieves. Altering the reaction conditions by changing the temperature and methanol WHSV led to further improvements in the propylene selectivity for CIT-17. A P/E ratio of 4.17 was reported for CIT-17, which is one of the highest P/E ratios recorded

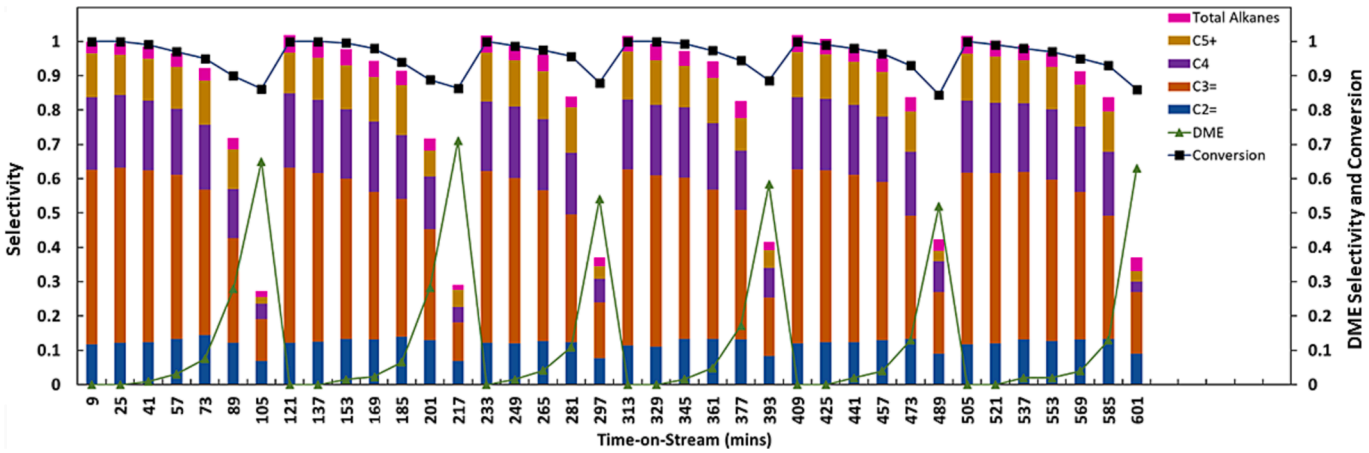

Fig. 6. Time-on-stream (TOS) plot of six consecutive reactions with CIT-17-4 at the optimized reaction conditions (350 °C and WHSV of 0.65 h^{-1}). (Note: multiply selectivity and conversion values by 100 to obtain them in percentages).

for this class of materials.

To rationalize the differences in the MTO behavior between these three frameworks, organic species retained in the cavities of the partially reacted catalysts were analyzed after 5 mins of reaction via dissolution of the molecular sieve and extraction of organic components. SAPO-34 samples retained mostly 4 MB, 5 MB, and 6 MB whereas SAPO-18 retained mostly 5 MB and 6 MB. CIT-17, on the other hand, comprised mostly of 3 MB and 4 MB, which are aromatic species that are typically associated with ethylene. Further investigation into the concentrations of the aromatic species in these catalysts revealed that CIT-17 materials accumulate aromatic species at a much lower rate than CHA and AEI. Therefore, by regulating the cage size and acid site density as well as strength of small-pore, cage-type molecular sieves, an enhancement in propylene selectivity can be achieved by increasing the contribution of the olefins cycle.

5. Personal acknowledgement

We are delighted to contribute to this special issue in honor of Professor Bruce C. Gates. One of us (M.E.D) first met Professor Gates during his initial visit to the University of Delaware when he was an assistant professor at Virginia Tech. From that time forward, Bruce has provided meaningful feedback to the Davis research program. It has been a pleasure to have had his insightful input. Professor Gates has a long history of providing leadership in heterogeneous catalysis, and he will be missed when he finishes his amazing career. Well done, Bruce, and best wishes.

CRediT authorship contribution statement

Faisal H. Alshafei: Conceptualization, Data curation, Formal analysis, Writing – original draft, Writing – review & editing. **Stacey I. Zones:** Supervision, Writing – review & editing. **Mark E. Davis:** Conceptualization, Funding acquisition, Supervision, Writing – review & editing.

Declaration of competing interest

The authors declare the following financial interests/personal relationships which may be considered as potential competing interests: A US patent application related to this work has been submitted, and the co-inventors are F.H.A. and M.E.D. S.I. Zones is an employee of the Chevron Corporation.

Data availability

The authors are unable or have chosen not to specify which data has been used.

Acknowledgements

The Chevron Energy and Technology Company provided financial support for this research. The authors gratefully acknowledge Dr. Sonjong Hwang for assistance with solid-state NMR and Dr. Nathan Dalleska (Resnick Water and Environment Laboratory at the California Institute of Technology) for assistance with the GC-MS experiments. FHA would like to thank Aramco R&D for financially supporting his graduate studies.

Appendix A. Supplementary data

Supplementary data to this article can be found online at https://doi.org/10.1016/j.cej.2024.149045.

References

[1] G. Hayes, M. Laurel, D. MacKinnon, T. Zhao, H.A. Houck, C.R. Becer, Polymers without Petrochemicals: Sustainable Routes to Conventional Monomers, Chem. Rev. 123 (2023) 2609–2734, https://doi.org/10.1021/acs.chemrev.2c00354.
[2] C.W. Fernelius, H. Wittcoff, R.E. Varnerin, Ethylene: The organic chemical industry's most important building block, J. Chem. Educ. 56 (1979) 385, https://doi.org/10.1021/ed056p385.
[3] I. Yarulina, A.D. Chowdhury, F. Meirer, B.M. Weckhuysen, J. Gascon, Recent trends and fundamental insights in the methanol-to-hydrocarbons process, Nature, Catalysis. 1 (2018) 398–411, https://doi.org/10.1038/s41929-018-0078-5.
[4] I. Amghizar, L.A. Vandewalle, K.M.V. Geem, G.B. Marin, New Trends in Olefin Production, Engineering 3 (2017) 171–178, https://doi.org/10.1016/J.ENG.2017.02.006.
[5] J.J.H.B. Sattler, J. Ruiz-Martinez, E. Santillan-Jimenez, B.M. Weckhuysen, Catalytic Dehydrogenation of Light Alkanes on Metals and Metal Oxides, Chem. Rev. 114 (2014) 10613–10653, https://doi.org/10.1021/cr5002436.
[6] T. Otroshchenko, Q. Zhang, E.V. Kondratenko, Enhancing Propene Formation in the Metathesis of Ethylene with 2-Butene at Close to Room Temperature over MoOx/SiO2 through Support Promotion with P, Cl, or S, ACS Catal. 11 (2021) 14159–14167, https://doi.org/10.1021/acscatal.1c04267.
[7] P. Tian, Y. Wei, M. Ye, Z. Liu, Methanol to Olefins (MTO): From Fundamentals to Commercialization, ACS Catal. 5 (2015) 1922–1938, https://doi.org/10.1021/acscatal.5b00007.
[8] C.A. Carrero, R. Schloegl, I.E. Wachs, R. Schomaecker, Critical Literature Review of the Kinetics for the Oxidative Dehydrogenation of Propane over Well-Defined Supported Vanadium Oxide Catalysts, ACS Catal. 4 (2014) 3357–3380, https://doi.org/10.1021/cs5003417.
[9] T. Lin, K. Gong, C. Wang, Y. An, X. Wang, X. Qi, S. Li, Y. Lu, L. Zhong, Y. Sun, Fischer-Tropsch Synthesis to Olefins: Catalytic Performance and Structure Evolution of Co2C-Based Catalysts under a CO2 Environment, ACS Catal. 9 (2019) 9554–9567, https://doi.org/10.1021/acscatal.9b02513.
[10] S. Chen, X. Chang, G. Sun, T. Zhang, Y. Xu, Y. Wang, C. Pei, J. Gong, Propane dehydrogenation: catalyst development, new chemistry, and emerging technologies, Chem. Soc. Rev. 50 (2021) 3315–3354, https://doi.org/10.1039/D0CS00814A.
[11] H. Yamazaki, H. Shima, H. Imai, T. Yokoi, T. Tatsumi, J.N. Kondo, Evidence for a "Carbene-like" Intermediate during the Reaction of Methoxy Species with Light Alkenes on H-ZSM-5, Angew. Chem. Int. Ed. 50 (2011) 1853–1856, https://doi.org/10.1002/anie.201007178.
[12] H.M. Torres Galvis, K.P. de Jong, Catalysts for Production of Lower Olefins from Synthesis Gas: A Review, ACS Catal. 3 (2013) 2130–2149, https://doi.org/10.1021/cs4003436.
[13] J.Q. Chen, A. Bozzano, B. Glover, T. Fuglerud, S. Kvisle, Recent advancements in ethylene and propylene production using the UOP/Hydro MTO process, Catal. Today 106 (2005) 103–107, https://doi.org/10.1016/j.cattod.2005.07.178.
[14] Y. Richardson, M. Drobek, A. Julbe, J. Blin, F. Pinta, Chapter 8 - Biomass Gasification to Produce Syngas, in: A. Pandey, T. Bhaskar, M. Stöcker, R. K. Sukumaran (Eds.), Recent Advances in Thermo-Chemical Conversion of Biomass, Elsevier, Boston, 2015, pp. 213–250, https://doi.org/10.1016/B978-0-444-63289-0.00008-9.
[15] Z. Ma, M.D. Porosoff, Development of Tandem Catalysts for CO2 Hydrogenation to Olefins, ACS Catal. 9 (2019) 2639–2656, https://doi.org/10.1021/acscatal.8b05060.
[16] A.M. Alamer, M. Ouyang, F.H. Alshafei, M.A. Nadeem, Y. Alsalik, J.T. Miller, M. Flytzani-Stephanopoulos, E.C.H. Sykes, V. Manousiouthakis, N.M. Eagan, Design of Dilute Palladium-Indium Alloy Catalysts for the Selective Hydrogenation of CO2 to Methanol, ACS Catal. 13 (2023) 9987–9996, https://doi.org/10.1021/acscatal.3c01861.
[17] X. Sun, S. Mueller, Y. Liu, H. Shi, G.L. Haller, M. Sanchez-Sanchez, A.C. van Veen, J.A. Lercher, On reaction pathways in the conversion of methanol to hydrocarbons on HZSM-5, J. Catal. 317 (2014) 185–197, https://doi.org/10.1016/j.jcat.2014.06.017.
[18] J.H. Kang, F.H. Alshafei, S.I. Zones, M.E. Davis, Cage-Defining Ring: A Molecular Sieve Structural Indicator for Light Olefin Product Distribution from the Methanol-to-Olefins Reaction, ACS Catal. 9 (2019) 6012–6019, https://doi.org/10.1021/acscatal.9b00746.
[19] J.H. Kang, R. Walter, D. Xie, T. Davis, C.-Y. Chen, M.E. Davis, S.I. Zones, Further Studies on How the Nature of Zeolite Cavities That Are Bounded by Small Pores Influences the Conversion of Methanol to Light Olefins, ChemPhysChem 19 (2018) 412–419, https://doi.org/10.1002/cphc.201701197.
[20] Y. Bhawe, M. Moliner-Marin, J.D. Lunn, Y. Liu, A. Malek, M. Davis, Effect of Cage Size on the Selective Conversion of Methanol to Light Olefins, ACS Catal. 2 (2012) 2490–2495, https://doi.org/10.1021/cs300558x.
[21] P. Ferri, C. Li, C. Paris, A. Rodríguez-Fernández, M. Moliner, M. Boronat, A. Corma, The Limits of the Confinement Effect Associated to Cage Topology on the Control of the MTO Selectivity, ChemCatChem 13 (2021) 1578–1586, https://doi.org/10.1002/cctc.202001760.
[22] P. Ferri, C. Li, C. Paris, A. Vidal-Moya, M. Moliner, M. Boronat, A. Corma, Chemical and Structural Parameter Connecting Cavity Architecture, Confined Hydrocarbon Pool Species, and MTO Product Selectivity in Small-Pore Cage-Based Zeolites, ACS Catal. 9 (2019) 11542–11551, https://doi.org/10.1021/acscatal.9b04588.
[23] P. Ferri, C. Li, R. Millán, J. Martínez-Triguero, M. Moliner, M. Boronat, A. Corma, Impact of Zeolite Framework Composition and Flexibility on Methanol-To-Olefins Selectivity: Confinement or Diffusion? Angew. Chem. Int. Ed. 59 (2020) 19708–19715, https://doi.org/10.1002/anie.202007609.

[24] I. Pinilla-Herrero, C. Márquez-Álvarez, E. Sastre, Complex relationship between SAPO framework topology, content and distribution of Si and catalytic behaviour in the MTO reaction, Catal. Sci. Technol. 7 (2017) 3892–3901, https://doi.org/10.1039/C7CY01250K.
[25] W. Dai, X. Wang, G. Wu, N. Guan, M. Hunger, L. Li, Methanol-to-Olefin Conversion on Silicoaluminophosphate Catalysts: Effect of Brønsted Acid Sites and Framework Structures, ACS Catal. 1 (2011) 292–299, https://doi.org/10.1021/cs200016u.
[26] M.A. Deimund, L. Harrison, J.D. Lunn, Y. Liu, A. Malek, R. Shayib, M.E. Davis, Effect of Heteroatom Concentration in SSZ-13 on the Methanol-to-Olefins Reaction, ACS Catal. 6 (2016) 542–550, https://doi.org/10.1021/acscatal.5b01450.
[27] F.H. Alshafei, Y. Park, S.I. Zones, M.E. Davis, Methanol-to-olefins catalysis on ERI-type molecular sieves: towards enhancing ethylene selectivity, J. Catal. 404 (2021) 620–633, https://doi.org/10.1016/j.jcat.2021.10.025.
[28] M. Dusselier, M.A. Deimund, J.E. Schmidt, M.E. Davis, Methanol-to-Olefins Catalysis with Hydrothermally Treated Zeolite SSZ-39, ACS Catal. 5 (2015) 6078–6085, https://doi.org/10.1021/acscatal.5b01577.
[29] Y. Ji, M.A. Deimund, Y. Bhawe, M.E. Davis, Organic-Free Synthesis of CHA-Type Zeolite Catalysts for the Methanol-to-Olefins Reaction, ACS Catal. 5 (2015) 4456–4465, https://doi.org/10.1021/acscatal.5b00404.
[30] J. Hua, X. Dong, J. Wang, C. Chen, Z. Shi, Z. Liu, Y. Han, Methanol-to-Olefin Conversion over Small-Pore DDR Zeolites: Tuning the Propylene Selectivity via the Olefin-Based Catalytic Cycle, ACS Catal. 10 (2020) 3009–3017, https://doi.org/10.1021/acscatal.9b05521.
[31] J. Xie, D.S. Firth, T. Cordero-Lanzac, A. Airi, C. Negri, S. Øien-Ødegaard, K. P. Lillerud, S. Bordiga, U. Olsbye, MAPO-18 Catalysts for the Methanol to Olefins Process: Influence of Catalyst Acidity in a High-Pressure Syngas (CO and H2) Environment, ACS Catal. 12 (2022) 1520–1531, https://doi.org/10.1021/acscatal.1c04694.
[32] P. Cnudde, R. Demuynck, S. Vandenbrande, M. Waroquier, G. Sastre, V. V. Speybroeck, Light Olefin Diffusion during the MTO Process on H-SAPO-34: A Complex Interplay of Molecular Factors, J. Am. Chem. Soc. 142 (2020) 6007–6017, https://doi.org/10.1021/jacs.9b10249.
[33] Z. Shi, A. Bhan, Tuning the ethylene-to-propylene ratio in methanol-to-olefins catalysis on window-cage type zeolites, J. Catal. 395 (2021) 266–272, https://doi.org/10.1016/j.jcat.2021.01.015.
[34] I.J. Castellanos-Beltran, G.P. Assima, J.-M. Lavoie, Effect of temperature in the conversion of methanol to olefins (MTO) using an extruded SAPO-34 catalyst, Frontiers of Chemical Science and Engineering 12 (2018) 226–238, https://doi.org/10.1007/s11705-018-1709-8.
[35] E. Borodina, H. Sharbini Harun Kamaluddin, F. Meirer, M. Mokhtar, A.M. Asiri, S. A. Al-Thabaiti, S.N. Basahel, J. Ruiz-Martinez, B.M. Weckhuysen, Influence of the Reaction Temperature on the Nature of the Active and Deactivating Species During Methanol-to-Olefins Conversion over H-SAPO-34, ACS Catal. 7 (2017) 5268–5281. doi: 10.1021/acscatal.7b01497.
[36] J. Zhong, J. Han, Y. Wei, Z. Liu, Catalysts and shape selective catalysis in the methanol-to-olefin (MTO) reaction, J. Catal. 396 (2021) 23–31, https://doi.org/10.1016/j.jcat.2021.01.027.
[37] I.M. Dahl, S. Kolboe, On the Reaction Mechanism for Hydrocarbon Formation from Methanol over SAPO-34: I. Isotopic Labeling Studies of the Co-Reaction of Ethene and Methanol, J. Catal. 149 (1994) 458–464, https://doi.org/10.1006/jcat.1994.1312.
[38] M. Hu, C. Wang, X. Gao, Y. Chu, G. Qi, Q. Wang, G. Xu, J. Xu, F. Deng, Establishing a Link Between the Dual Cycles in Methanol-to-Olefins Conversion on H-ZSM-5: Aromatization of Cycloalkenes, ACS Catal. 10 (2020) 4299–4305, https://doi.org/10.1021/acscatal.0c00838.
[39] X. Sun, S. Mueller, H. Shi, G.L. Haller, M. Sanchez-Sanchez, A.C. van Veen, J. A. Lercher, On the impact of co-feeding aromatics and olefins for the methanol-to-olefins reaction on HZSM-5, J. Catal. 314 (2014) 21–31, https://doi.org/10.1016/j.jcat.2014.03.013.
[40] A. Hwang, D. Prieto-Centurion, A. Bhan, Isotopic tracer studies of methanol-to-olefins conversion over HSAPO-34: The role of the olefins-based catalytic cycle, J. Catal. 337 (2016) 52–56, https://doi.org/10.1016/j.jcat.2016.01.021.
[41] A. Hwang, B.A. Johnson, A. Bhan, Mechanistic study of methylbenzene dealkylation in methanol-to-olefins catalysis on HSAPO-34, J. Catal. 369 (2019) 86–94, https://doi.org/10.1016/j.jcat.2018.10.022.
[42] J. Goetze, F. Meirer, I. Yarulina, J. Gascon, F. Kapteijn, J. Ruiz-Martínez, B. M. Weckhuysen, Insights into the Activity and Deactivation of the Methanol-to-Olefins Process over Different Small-Pore Zeolites As Studied with Operando UV–vis Spectroscopy, ACS Catal. 7 (2017) 4033–4046, https://doi.org/10.1021/acscatal.6b03677.
[43] Q. Peng, G. Wang, Z. Wang, R. Jiang, D. Wang, J. Chen, J. Huang, Tuning Hydrocarbon Pool Intermediates by the Acidity of SAPO-34 Catalysts for Improving Methanol-to-Olefins Reaction, ACS Sustainable Chem. Eng. 6 (2018) 16867–16875, https://doi.org/10.1021/acssuschemeng.8b04210.
[44] S. Teketel, W. Skistad, S. Benard, U. Olsbye, K.P. Lillerud, P. Beato, S. Svelle, Shape Selectivity in the Conversion of Methanol to Hydrocarbons: The Catalytic Performance of One-Dimensional 10-Ring Zeolites: ZSM-22, ZSM-23, ZSM-48, and EU-1, ACS Catal. 2 (2012) 26–37, https://doi.org/10.1021/cs200517u.
[45] S. Ilias, R. Khare, A. Malek, A. Bhan, A descriptor for the relative propagation of the aromatic- and olefin-based cycles in methanol-to-hydrocarbons conversion on H-ZSM-5, J. Catal. 303 (2013) 135–140, https://doi.org/10.1016/j.jcat.2013.03.021.
[46] R.L. Smith, S. Svelle, P. del Campo, T. Fuglerud, B. Arstad, A. Lind, S. Chavan, M. P. Attfield, D. Akporiaye, M.W. Anderson, CHA/AEI intergrowth materials as catalysts for the Methanol-to-Olefins process, Appl. Catal.A: General 505 (2015) 1–7, https://doi.org/10.1016/j.apcata.2015.06.027.
[47] R. Martínez-Franco, Z. Li, J. Martínez-Triguero, M. Moliner, A. Corma, Improving the catalytic performance of SAPO-18 for the methanol-to-olefins (MTO) reaction by controlling the Si distribution and crystal size, Catal. Sci. Technol. 6 (2016) 2796–2806, https://doi.org/10.1039/C5CY02298C.
[48] N. Martín, Z. Li, J. Martínez-Triguero, J. Yu, M. Moliner, A. Corma, Nanocrystalline SSZ-39 zeolite as an efficient catalyst for the methanol-to-olefin (MTO) process, Chem. Commun. 52 (2016) 6072–6075, https://doi.org/10.1039/C5CC09719C.
[49] S. Hu, J. Shan, Q. Zhang, Y. Wang, Y. Liu, Y. Gong, Z. Wu, T. Dou, Selective formation of propylene from methanol over high-silica nanosheets of MFI zeolite, Appl. Catal.A: General 445–446 (2012) 215–220, https://doi.org/10.1016/j.apcata.2012.08.032.
[50] L. Lin, M. Fan, A.M. Sheveleva, X. Han, Z. Tang, J.H. Carter, I. da Silva, C.M. A. Parlett, F. Tuna, E.J.L. McInnes, G. Sastre, S. Rudić, H. Cavaye, S.F. Parker, Y. Cheng, L.L. Daemen, A.J. Ramirez-Cuesta, M.P. Attfield, Y. Liu, C.C. Tang, B. Han, S. Yang, Control of zeolite microenvironment for propene synthesis from methanol, Nat. Commun. 12 (2021) 822, https://doi.org/10.1038/s41467-021-21062-1.
[51] S. Hu, Y. Gong, Q. Xu, X. Liu, Q. Zhang, L. Zhang, T. Dou, Highly selective formation of propylene from methanol over high-silica EU-1 zeolite catalyst, Catal. Commun. 28 (2012) 95–99, https://doi.org/10.1016/j.catcom.2012.08.011.
[52] X. Zhao, L. Wang, J. Li, S. Xu, W. Zhang, Y. Wei, X. Guo, P. Tian, Z. Liu, Investigation of methanol conversion over high-Si beta zeolites and the reaction mechanism of their high propene selectivity, Catal. Sci. Technol. 7 (2017) 5882–5892, https://doi.org/10.1039/C7CY01804E.
[53] Y. Ji, J. Birmingham, M.A. Deimund, S.K. Brand, M.E. Davis, Steam-dealuminated, OSDA-free RHO and KFI-type zeolites as catalysts for the methanol-to-olefins reaction, Microporous and Mesoporous Materials 232 (2016) 126–137, https://doi.org/10.1016/j.micromeso.2016.06.012.
[54] M. Yang, B. Li, M. Gao, S. Lin, Y. Wang, S. Xu, X. Zhao, P. Guo, Y. Wei, M. Ye, P. Tian, Z. Liu, High Propylene Selectivity in Methanol Conversion over a Small-Pore SAPO Molecular Sieve with Ultra-Small Cage, ACS Catal. 10 (2020) 3741–3749, https://doi.org/10.1021/acscatal.9b04703.
[55] G.W. Noble, P.A. Wright, Å. Kvick, The templated synthesis and structure determination by synchrotron microcrystal diffraction of the novel small pore magnesium aluminophosphate STA-2 †, J. Chem. Soc., Dalton Trans. (1997) 4485–4490, https://doi.org/10.1039/A705091G.
[56] M. Castro, V.R. Seymour, D. Carnevale, J.M. Griffin, S.E. Ashbrook, P.A. Wright, D. C. Apperley, J.E. Parker, S.P. Thompson, A. Fecant, N. Bats, Molecular Modeling, Multinuclear NMR, and Diffraction Studies in the Templated Synthesis and Characterization of the Aluminophosphate Molecular Sieve STA-2, J. Phys. Chem. C 114 (2010) 12698–12710, https://doi.org/10.1021/jp104120y.
[57] V.R. Seymour, E.C.V. Eschenroeder, P.A. Wright, S.E. Ashbrook, An NMR crystallographic approach to monitoring cation substitution in the aluminophosphate STA-2, Solid State Nuclear Magnetic Resonance 65 (2015) 64–74, https://doi.org/10.1016/j.ssnmr.2014.10.007.
[58] Y. Li, Y. Huang, J. Guo, M. Zhang, D. Wang, F. Wei, Y. Wang, Hierarchical SAPO-34/18 zeolite with low acid site density for converting methanol to olefins, Catal. Today 233 (2014) 2–7, https://doi.org/10.1016/j.cattod.2014.03.038.
[59] P. Wang, A. Lv, J. Hu, J. Xu, G. Lu, The synthesis of SAPO-34 with mixed template and its catalytic performance for methanol to olefins reaction, Microporous Mesoporous Mater. 152 (2012) 178–184, https://doi.org/10.1016/j.micromeso.2011.11.037.
[60] Y. Wang, S.-L. Chen, Y.-J. Jiang, Y.-Q. Cao, F. Chen, W.-K. Chang, Y.-L. Gao, Influence of template content on selective synthesis of SAPO-18, SAPO-18/34 intergrowth and SAPO-34 molecular sieves used for methanol-to-olefins process, RSC Adv. 6 (2016) 104985–104994, https://doi.org/10.1039/C6RA23048B.
[61] B. Shen, X. Chen, X. Fan, H. Xiong, H. Wang, W. Qian, Y. Wang, F. Wei, Resolving atomic SAPO-34/18 intergrowth architectures for methanol conversion by identifying light atoms and bonds, Nat. Commun. 12 (2021) 2212, https://doi.org/10.1038/s41467-021-22438-z.
[62] M.-A. Djieugoue, A.M. Prakash, L. Kevan, Electron Spin Resonance and Electron Spin−Echo Modulation Studies of Synthesized NiAPSO-34 Molecular Sieve and Comparison with Ion-Exchanged NiH−SAPO-34 Molecular Sieve, J. Phys. Chem. B 103 (1999) 804–811, https://doi.org/10.1021/jp9823897.
[63] S. Ashtekar, S.V.V. Chilukuri, A.M. Prakash, D.K. Chakrabarty, Small Pore Aluminum Phosphate Molecular Sieves with Chabazite Structure: Incorporation of Manganese in the Structures -34 and -44, J. Phys. Chem. 100 (1996) 3665–3670, https://doi.org/10.1021/jp951800c.
[64] S. Ashtekar, S.V.V. Chilukuri, A.M. Prakash, C.S. Harendranath, D.K. Chakrabarty, Small Pore Aluminum Phosphate Molecular Sieves with Chabazite Structure: Incorporation of Cobalt in the Structures -34 and -44, J. Phys. Chem. 99 (1995) 6937–6943, https://doi.org/10.1021/j100018a027.
[65] D. Fan, P. Tian, S. Xu, Q. Xia, X. Su, L. Zhang, Y. Zhang, Y. He, Z. Liu, A novel solvothermal approach to synthesize SAPO molecular sieves using organic amines as the solvent and template, J. Mater. Chem. 22 (2012) 6568–6574, https://doi.org/10.1039/C2JM15281A.
[66] J. Chen, P.A. Wright, J.M. Thomas, S. Natarajan, L. Marchese, S.M. Bradley, G. Sankar, C.R.A. Catlow, P.L. Gai-Boyes, SAPO-18 Catalysts and Their Broensted Acid Sites, J. Phys. Chem. 98 (1994) 10216–10224, https://doi.org/10.1021/j100091a042.
[67] F.H. Alshafei, J.H. Kang, S.J. Cho, M.E. Davis, Synthesis and Characterization of Silicoaluminophosphate CIT-16P and Its Transformation to SAPO-17, Inorg. Chem. 62 (2023) 6065–6075, https://doi.org/10.1021/acs.inorgchem.2c04539.
[68] S. ul H. Bakhtiar, S. Ali, X. Wang, F. Yuan, Z. Li, Y. Zhu, Synthesis of sub-micrometric SAPO-34 by a morpholine assisted two-step hydrothermal route and

its excellent MTO catalytic performance, Dalton Trans. 48 (2019) 2606–2616. doi: 10.1039/C8DT04559C.
[69] H. He, J. Klinowski, Solid-state NMR studies of the aluminophosphate molecular sieve AlPO4-18, J. Phys. Chem. 97 (1993) 10385–10388, https://doi.org/10.1021/j100142a020.
[70] Z. Duan, N. Wang, H. Xu, P. Wu, Structural Transformation-Involved Synthesis of Nanosized ERI-Type Zeolite and Its Catalytic Property in the MTO Reaction, Inorg. Chem. 61 (2022) 8066–8075, https://doi.org/10.1021/acs.inorgchem.2c00914.
[71] S.T. Wilson, R.W. Broach, C.S. Blackwell, C.A. Bateman, N.K. McGuire, R. M. Kirchner, Synthesis, characterization and structure of SAPO-56, a member of the ABC double-six-ring family of materials with stacking sequence AABBCCBB, Microporous Mesoporous Mater. 28 (1999) 125–137, https://doi.org/10.1016/S1387-1811(98)00293-5.
[72] I. Miletto, C. Ivaldi, G. Paul, S. Chapman, L. Marchese, R. Raja, E. Gianotti, Hierarchical SAPO-34 Architectures with Tailored Acid Sites using Sustainable Sugar Templates, ChemistryOpen. 7 (2018) 297–301, https://doi.org/10.1002/open.201800001.